# GMD manuscript #2020-404: replies to the reviews

Michael Olesik, Sylwester Arabas and co-authors

July 2021

First, let us thank all three reviewers for their valuable critique and feedback. Below, we provide point-by-point replies to all comments. Quoted text of the reviews is typeset in teal and with larger margins.
A revised manuscript with changes automatically highlighted using the latexdiff tool is enclosed with additions marked with blue color and deleted text in red. Additions to the bibliography are not color-highlighted, but all references to new bibliography items are within blue-underlined blocks in the text.
The key change in the manuscript is the introduction of an entirely new section (numbered 3 in the revised manuscript) covering two-dimensional simulations in which one of the dimension corresponds to the particle size and the other to vertical displacement in a column of air. These simulations feature coupling between particle growth and ambient supersaturation dynamics. This addresses the main point of all three reviews of overly simplified test case employed.

## comments by Josef Schröttle, 24 Feb 2021

> This study introduces a new Python library for advection of geophysical flows with the MPDATA scheme. More specifically, it concentrates on the broadening of cloud droplet distributions due to advection and compares those distributions to analytically derived functions. It is based on previous work by the authors in a C++ library and numerous studies that have been conducted since the 1980s up to now. The paper is clearly written in the introduction, the methodology, and results sections. The reader would profit from a more fluent overview of the background literature in this work (in section 1.2),

Several correction to punctuation, the usage of articles and sentence shortening has hopefully improved Section 1.2.

> ... as well as a brief motivation why this is such important work especially in the context of clouds. A short suggestion of how to incorporate this is given by the reviewer. Also, a brief description of the software for interested users would be very helpful. Overall, this work is unique in its focus on comparing 2-3 advection

schemes in the context of cloud dynamics and could be a basis for many future applications after major revision.

First general comments from my side:

•To give a brief motivation, why your work is so important, I would refer to clouds in climate research, e.g.: Climate goals and computing the future of clouds, Nature Climate Change volume 7, pages 3–5 (2017) or a more recent publication

The background section was extended following the reviewer's suggestion including a reference to the Schneider et al. 2017 paper.

•How do your simulations evolve in time? Besides the cloud distributions you show in Fig. 1ff, I would like to see Hovmoeller diagrams of cloud distributions of selected experiments to see their temporal evolution.

The new section covering two-dimensional simulations features two figures addressing this point. The newly introduced Figure 11 depicts the temporal evolution of the spectral width parameter $d$, while the new Figure 10 depicts actual binned size spectra at each level of the vertical grid conveying analogous information as a Hovmöller spectral-temporal diagram.

•Have you tried more advection schemes besides: upwind, mpdata 2, mpdata 3?

A comparison with other techniques, in particular with the Lagrangian (moving-sectional, particle-reolved) representation is planned for a follow up study. The concept for this paper is to constitute a guide across different aspects of the MPDATA algorithm which need to (or can optionally) be, taken into account while addressing the particular problem of particle condensational growth.

•You should point out the clear improvement of MPDATA compared to upwind scheme.

The newly introduced Fig. 12 aptly highlights this improvement depicting the robustness in which application of even a single corrective iteration of MPDATA basically halves the spectral width of the simulated droplet spectra.

•What are the initial conditions in your simulation? What noise do you use?

The initial condition has been specified in section 1.5, in particular through the equation 1.6 (initial particle spectrum) and the numerical parameters given below (timestep, grid layout). No noise considered.

•Please provide a comparison for the plot of mixing ratios versus Rd (Fig. 9) to observations from nature or experiments. Again, state explicitly in the caption of Fig. 9, what Rd symbolizes: Radius of ...

$R_d$ symbolizes the analytical-to-numerical ratio of the values of the droplet spectral width $d$. The misleading $R_{\text{disp}}$ vs. $R_d$ naming has been unified and the figure cation includes the definition now instead of a reference to an equation.
The discussion of the newly introduced Figure 11 features a reference to observations.

> •The error overview plots Fig. A1ff are a very interesting way to compare advection schemes and experiments, efficiently. Why do you not pull those into the results section for selected experiments? Is the truth for computing the error the analytical model?

Yes, the error measure is based on the analytical solution (as indicated in eq. A1). The highlight of the polar plots presented in the appendix is the Courant number dependence of the rate of convergence. It is of importance when devising case study setups or developing adaptive timestepping criteria - both relevant, yet of secondary relevance to the storyline of the paper, hence presented in an appendix.

> •You should - point out in the conclusion, that this study can be a basis for future work.

The last paragraph of the conclusions now outlines the path towards four-dimensional MPDATA solver capable of integrating bin microphysics dynamics in 3D CFD framework.

> I am looking forward to providing more detailed comments in the next iteration of this manuscript. For now, some technical comments:
>
> (a) Fig.1:... those are cloud droplet distributions, right? Please state this, explicitly.

It is now clarified in the caption that the plot depicts particle number densities.

> (b) Fig.1: Can you provide the analytical functions for the distributions & its derivations?

It is given with an outline of derivation when introducing eq. 2.5, with reference to the .

> (c) A better description of the Python library is required for interested readers to repeat your experiments. You can do that either in README file on github or in a section of this paper.

The PyMPDATA README file has undergone significant expansion including addition of new examples and inclusion of sample code in Julia and Matlab. The public API of the library is now published along with annotations at `https://atmos-cloud-sim-uj.github.io/PyMPDATA`. Submission of a short paper to the Journal of Open Source Software outlining the package features is planned.

## comments by Anonymous Referee #2, 01 May 2021

> This study examined performance of various MPDATA variants in solving drop size distribution evolution by condensation. The authors reviewed many previous studies in the context of improving MPDATA and showed that MPDATA with three anti-diffusive iterations, third order term, infinite gauge, and the non-oscillatory option reduces the numerical diffusion to roughly a tenth compared to that of the upwind scheme, although it requires $\sim$ 10 times longer than the upwind scheme.

The computational cost footprint is now highlighted in the abstract to clarify that the increased accuracy comes at a trade off.

> Although this study examined the performance of MPDATA variants systematically, I would raise two serious problems this study bears. At the current stage, my recommendation is to reject the manuscript for publishing on GMD, and encouraging the authors to improve the manuscript accordingly.
>
> 1. Somewhat outdated
>
> I can find several recent papers closely related to the topic this study focuses on: Morrison et al. (2018, doi: 10.1175/JAS-D-18-0055.1), Pardo et al. (2020, doi:10.1175/JAS-D-20-0099.1), and Lee et al. (2021, doi:10.1175/JAS-D-20-0213.1). All those papers already pointed out that drop condensation itself can be sufficiently converged with better schemes or better designed grids, but it is the condensation w/ vertical advection or w/ collision-coalescence that causes serious problems. Furthermore, those studies utilized LES model results in explaining their results, whereas this study only showed the box model results. This study clearly exhibited the performance of MPDATA variants in solving drop condensation, but only the convergence test in solving drop condensation is somewhat outdated compared to the studies I mentioned. I strongly suggest the authors to improve their study by including vertical advection, collision-coalescence, and/or something we do not know its effects.

The newly added section featuring single-column case study involves vertical advection. All three recent papers mentioned are now referenced commented on.

> 2. Experimental setting
>
> In the authors' experimental setting, supersaturation is fixed so the liquid water content increases up to 10 g kg–1, which is almost unrealistic except for tropical cyclones. I strongly suggest the authors to modify the experimental setting so the results become more realistic. For example, Morrison et al. (2018) and Lee et al. (2021) fixed the vertical velocity to be 1 m s–1 for  20 min rather than fixed the supersaturation.

The newly added single-column test case features supersaturation dynamics coupling with the particle growth.
The original box model setup was kept as is. Despite somewhat unrealistic range of liquid water content it allows for performing the convergence analysis across a wide range of grid- and timesteps.

## comments by Anonymous Referee #3, 04 May 2021

> This manuscript examines the fidelity of various flavors of the MPDATA advection scheme for solving condensation of the drop size distribution. The writing style is clear and concise, the historical review of bin scheme and MPDATA development was illuminating, and the figures were simple and easy to understand. That said, the study suffers from a few key flaws that lead me to suggest the paper be rejected.
>
> First, the authors recognize that the difficulty of numerically modeling condensation/evaporation is that drop growth processes (in the mass dimension) are fundamentally coupled to spatial advection. Yet the test case, which if I understand correctly was chosen because a reference analytical solution can be obtained, either did not include a spatial advection component or this was not discussed. Morrison et al. (2018) and Lee et al. (2021) both point out that satisfactory solutions can be obtained by a number of schemes in the absence of transport; it is when they are coupled that special consideration must be taken.

The newly added section (number 3 in the revised manuscript) addresses this point by considering a two-dimensional problem with both the spectral and spatial transport considered simultaneously.

> Secondly, the physical feasibility of the test case is dubious; in any warm cloud, a mass mixing ratio of 10 g/kg is nigh impossible.

The choice of the test case for the box model simulations was motivated partly by the aim of performing the convergence analysis presented in the appendix which covers a wide range of grid- and timesteps.

> Finally, another important aspect (in particular, of Lee et al., 2021) was not covered: the effect of refining grid spacing vs. refining algorithm formulation.

This point is addressed in the analysis presented in the newly introduced Fig. 12 where results with different number of MPDATA iterations are presented for an array of $\Delta t$, $\Delta r$ and $\Delta z$ settings.

> These three factors combined leave me with the impression that this study, while rigorous, is not relevant to the current state of the field.
>
> I strongly encourage the authors to reconsider the paper by formulating a test case that would demonstrate the relevance of the algorithms tested in dynamical models, and evaluating the trade-off of increased algorithmic accuracy versus refined size grid.

We have followed the request introducing the single-column test case which covers both the vertical transport aspect as well as the supersaturation dynamics coupling.

Let us close this reply by expressing again our thanks for the reviewers' feedback what is also expressed in the acknowledgments section in the revised text.

# On numerical broadening of particle size spectra: a condensational growth study using PyMPDATA 1.0

Michael Olesik[1], Sylwester Arabas[1], Jakub Banaśkiewicz[1], Piotr Bartman[1], Manuel Baumgartner[2,3], and Simon Unterstrasser[4]

[1]Jagiellonian University, Kraków, Poland
[2]Zentrum für Datenverarbeitung, Johannes Gutenberg University Mainz, Germany
[3]Institute for Atmospheric Physics, Johannes Gutenberg University Mainz, Germany
[4]German Aerospace Center (DLR), Oberpfaffenhofen, Germany

**Correspondence:** Michael Olesik (michael.olesik@doctoral.uj.edu.pl)

**Abstract.** ~~The~~ This work discusses the ~~diffusional~~ numerical aspects of representing the diffusional (condensational) growth in particulate systems such as atmospheric clouds. It focuses on the Eulerian modeling approach in which the evolution of the probability density function describing the particle size spectrum is carried out using a fixed-bin discretization ~~. The~~ (so-called "bin" microphysics). The numerical diffusion problem inherent to the employment of the fixed-bin discretization in the numerical solution of the arising transport problem is scrutinized. ~~The work focuses~~ Focus is on the applications of MPDATA family of numerical schemes. Several MPDATA variants are explored including: infinite-gauge, non-oscillatory, third-order-terms and recursive antidiffusive correction (double pass donor cell, DPDC) options. Methodology for handling coordinate transformations associated with both particle size distribution variable choice and numerical grid layout are expounded. The study uses PyMPDATA - a new open-source Python implementation of MPDATA. Analysis of the performance of the scheme for different discretization parameters and different settings of the algorithm is performed using: (i) an analytically solvable ~~test case pertinent to condensational growth of cloud droplets. The analysis covers spatial~~ box-model test case, and (ii) the single-column "KiD" test case in which the size-spectral advection due to condensation is solved simultaneously with the spatial advection in the vertical physical coordinate, and in which the supersaturation evolution is coupled with the droplet growth through water mass budget. The single-column problem involves numerical solution of a two-dimensional advection problem (spectral and spatial dimensions). The discussion presented in the paper covers spatial (i.e. size-spectral) and temporal convergence, computational cost, conservativeness and quantification of the numerical broadening of the particle size spectrum. ~~Presented results~~ The box-model simulations demonstrate that, for the problem considered, even a tenfold decrease of the spurious numerical spectral broadening can be obtained by a proper choice of the MPDATA variant (maintaining the same spatial and temporal resolution)~~.~~ , yet at an increased computational cost. Analyses using the single-column test case reveal that the width of the droplet size spectrum is affected by numerical diffusion pertinent to both spatial and spectral advection. Application of even a single corrective iteration of MPDATA robustly decreases the relative dispersion of the droplet spectrum, roughly by a factor of two at the levels of maximal liquid water content.

# 1 Introduction

## 1.1 Motivation and outline

The focus of this paper is on the problem of predicting the particle size evolution for a population of droplets undergoing diffusional growth. Embracing continuous description of the particle size spectrum using a number density function, the problem can be stated using a population-balance equation expressing conservation of number of particles. Herein, the numerical solution of the problem using the MPDATA family of finite difference schemes originating in Smolarkiewicz (1983, 1984) is discussed. MPDATA stands for Multidimensional Positive Definite Advection Transport Algorithm and is a higher-order iterative extension of the forward-in-time upwind scheme.

MPDATA features a variety of options allowing to pick an algorithm variant appropriate to the problem at hand. This work highlights the importance of MPDATA algorithm variant choice for the resultant spectral broadening of the particle size spectrum.

The term spectral broadening refers to the increasing width of the droplet spectrum during the lifetime of a cloud, which may be associated with both physical mechanisms (mixing, turbulence) as well as spurious artifacts stemming from the employed numerical solution technique.

Cloud simulations with detailed treatment of droplet microphysics face a twofold challenge in prognosing the droplet spectrum width. First, it is challenging to model and numerically represent the subtleties of condensational growth (e.g., Arabas and Shima, 2017; Yang et al., 2018), even more so when considering the interplay between particle population dynamics and supersaturation fluctuations (e.g., Jeffery et al., 2007; Abade et al., 2018). Second, the discretization strategies employed in representing the particle size spectrum and its evolution are characterized by inherent limitations which constrains the fidelity of spectral width predictions (e.g., Arabas and Pawlowska, 2011; Morrison et al., 2018). Finally, corroboration of spectral width estimates from both theory and modeling against experimental data faces the problems of instrumental broadening inherent to the measurement techniques (e.g. Devenish et al., 2012, sec. 3.2) and the problem of sampling volume choice (e.g., Kostinski and Jameson, 2000).

The width of the spectrum plays a key role in the determination of both the droplet collision probabilities Grabowski and Wang (2013) and the characteristics relevant for radiative-transfer (Chandrakar et al., 2018). These in turn are reflected in parameterisations of cloud processes in large scale models. Taking climate timescale simulation as an example, the representation of clouds remains the largest source of uncertainty there (Schneider et al., 2017). The parameterisations used in climate models are developed based on smaller-scale simulations involving particle size-spectrum dynamics. Consequently, it is of high interest to disentangle the size effects on the droplet spectrum that come from the exact solution of the governing equation or are a consequence of the numerical discretization (i.e. numerical diffusion).

The following introductory subsections start with a literature review of applications of finite-difference schemes, and MPDATA in particular, to the problem of condensational growth of population of particles.

Section 2 ~~contains~~ focuses on a simple box-model test case and serves as a tutorial on MPDATA variants ~~and is~~ (limited to one-dimensional homogeneous advection of a positive-sign signal). It is presented with the aim of gathering information

that is scattered across works focusing on more complex computational fluid dynamics applications of MPDATA. Example simulations employing an analytically solvable test case pertaining to the evolution of cloud droplet size spectrum in a cumulus cloud is used to depict the effects on numerical broadening from enabling the discussed algorithm variants. An analysis of the computational cost of different algorithm variants is carried out and corroborated with previously published data. While comprehensive from the point of view of the considered problem of diffusional growth, the presented material merely hints the versatility of the algorithm. For a proper review of MPDATA family of algorithms highlighting the multi-dimensional aspects and its multifaceted applications, see Margolin and Smolarkiewicz (1998); Smolarkiewicz (2006); Kühnlein and Smolarkiewicz (2017).

Section ~~?? documents analyses of spectral broadening and mass conservativeness. An analysis of the computational cost of different algorithm variants is carried out and corroborated with previously published data~~3 covers application of MPDATA for coupled size-spectral and spatial advection in a single-column kinematic setup from Shipway and Hill (2012). First, the methodology to handle the spectral-spatial liquid water advection problem taking into account the coupling with the vapour field is detailed. Second, the results obtained using different MPDATA variants are discussed focusing on the measures of spectral broadening.

Section 4 concludes the work with a summary of findings.

Appendix A contains convergence analysis based on results of multiple simulations using the embraced box-model test case run with different temporal and spatial (size-spectral) resolutions.

### 1.2 Background

There exist two contrasting approaches for modeling the evolution of cloud droplet size spectrum (see Grabowski, 2020, for a review): Eulerian (~~fixed bin~~fixed-bin) and the Lagrangian (~~particle based or moving bin~~moving-bin or particle-based). The Lagrangian approach has the advantages of: (i) simplicity of formulation (no need to define particle-level properties and processes as gridded continuous fields), (ii) lack of discretization-related artifacts such as numerical diffusion associated with solving PDEs, (iii) facilitation of tracking multiple particle attributes such as the amount of solute required for modeling activation. On the other hand, there are inherent challenges in using the particles-based framework: (i) ensuring proper sampling of physical and parameter space, (ii) handling load-balancing in distributed memory environments, (iii) solvability of resultant stiff ODE systems. Overall, while the Lagrangian methods are the focus of active research and development (Grabowski et al., 2019), the Eulerian schemes have been predominantly used in large scale modeling (Khain et al., 2015), due to their consistency with the fluid advection dynamics description and due to robust algorithms for representing particle collisions.

Following Liu et al. (1997) and Morrison et al. (2018), the earliest documented study employing the Eulerian numerics for condensational growth of a continuous size distribution representing a population of particles is that of Kovetz and Olund (1969) (whereas several earlier works starting with the seminal study of Howell (1949) utilized the Lagrangian ~~approaches~~approach). The numerical scheme proposed in Kovetz and Olund (1969, eq. (10)) resembles an upwind algorithm being explicit in time and orienting the finite-difference stencil differently for condensation and evaporation.

Likely one of the first discussions of numerical broadening of the spectrum can be found in Brown (1980) where the numerical scheme from Kovetz and Olund (1969) was improved in several ways, including sampling of the drop growth rate at the bin boundaries (as is done ~~here). Their~~ herein). The study also covers quantification of the error of the method by comparisons to analytic solutions.

In Tsang and Brock (1982), the authors point out that upwind differencing is not suitable for aerosol growth calculations for its unacceptable numerical diffusion. Noteworthy, the study includes considerations of the Kelvin effect of surface tension on the drop growth (not considered herein).

The first mention of ~~application of MPDATA~~ an application of the MPDATA scheme for the problem of condensational growth can be found already in Smolarkiewicz (1984)~~where the~~ . The problem is given as an example where the divergent-flow option of the algorithm may be applicable (see sect. 2.6 below).

In Tsang and Korgaonkar (1987), which is focused on the evaporation of an "aerosol cloud", MPDATA is used as a predictor step followed by a corrective step using a Galerkin finite element solver. In two subsequent studies from the same group (Tsang and Rao, 1988, 1990), MPDATA is compared with other algorithms in terms of ~~mass conservation, number conservation~~ conservativeness and computational cost. In Tsang and Rao (1988), the basic 3-iteration MPDATA is used~~,~~ ~~although interestingly~~ . Interestingly, it is noted there that "*If the antidiffusion velocities are increased by some factor between 1.04 and 1.08, use of [corrective iteration] only once can reduce 50% of the computing time [...] without much sacrifice of accuracy*". In conclusions, the authors praise MPDATA for providing narrow size distributions. At the same time, it is pointed out that MPDATA performs worse than upwind in terms of ~~mass conservation or~~ mean radius prediction accuracy.

The "Aerosol Science: Theory and Practice" book of Williams and Loyalka (1991) contains a section ~~on MPDATA within Chapter 5 focusing~~ (5.19) on MPDATA (termed "Smolarkiewicz method") within a chapter focused on the methods of solving the dynamic equation describing aerosol spectrum evolution. The basic variant of MPDATA (Smolarkiewicz, 1983) is presented with an outline of its derivation.

In Kostoglou and Karabelas (1995) and Dhaniyala and Wexler (1996), the authors mention that MPDATA has the potential to reduce errors in particle size computations. The latter work lists high computational cost among drawbacks in using the algorithm that led to discarding the scheme from the presented comparison.

In Morrison et al. (2018), a comparison of different numerical schemes for condensational growth problem is performed. Both fixed-, and moving-bin approaches are compared, including the non-oscillatory variant of MPDATA (referred to as MPDG therein). MPDATA is reported to produce significant numerical diffusion and spectral broadening relative to all other methods. Intriguingly, as can be seen in Fig. 7 therein, the broad spectrum in the results obtained with MPDATA appears already at the very beginning of the simulations~~presented (~~, at the altitude of 20$\mathrm{m}$ out of 520$\mathrm{m}$ of simulated displacement of an air parcel~~)~~. Overall, the discussion in Morrison et al. (2018), which has prompted further analyses presented in Hernandéz Pardo et al. (2020) and Lee et al. (2021), focuses on the issue of spectral broadening from the vertical numerical diffusion highlighting that, in principle, the problem is a four-dimensional transport problem (three spatial dimensions and the spectral dimension).

In Wei et al. (2020), MPDATA is employed for integrating droplet spectrum evolution for comparison with a Lagrangian scheme. The work concludes that the spurious broadening of the spectrum cannot be alleviated even with a grid composed of 2000 (sic!) size bins.

Noteworthy, none of the works mentioned above discussed coordinate transformations to non-linear grid layouts with MPDATA (a discussion of handling non-uniform mesh with upwind scheme can be found in Li et al., 2017, Appendix A). Wei et al. (2020) and Morrison et al. (2018) are the only works mentioning other than basic flavor of the scheme, yet only the non-oscillatory option was considered. Herein, the applicability of multiple variants of MPDATA and their combinations is expounded highlighting their robustness for solving the condensational growth problem.

### 1.3 Governing equations

To describe the conservation of particle number $N$ under the evolution of the particle size spectrum $n_p(p) = \frac{dN}{dp}$ ($n$ denoting number density as a function of particle size parameter $p$ such as radius or volume), one may take the one-dimensional continuity equation (i.e., Liouville equation expressing the conservation of probability, for discussion see Hulburt and Katz, 1964), in a generalized coordinate system:

$$\partial_t(Gn_p) + \partial_x(uGn_p) = 0, \tag{1.1}$$

where $G \equiv G(x)$ represents the coordinate transformation from $p$ to $x$, $x$ being an equidistant mesh coordinate used in the numerical solution; $n_p \equiv n_p(p(x))$ being number density function and $u \equiv u(x)$ denoting the pace of particle growth in the chosen coordinate $x$. The coordinate transformation term $G$ may play a twofold role in this context. First, there is a degree of freedom in the choice of the particle-size parameter used as the coordinate (i.e., the argument $p$ of the density function $n(p)$). For the chosen coordinates $p \in [r, s \sim r^2, v \sim r^3]$, the appropriate distributions will be $n_r(r)$, $n_s(s)$ and $n_v(v)$ where $s = 4\pi r^2$ and $v = 4/3\pi r^3$ denote particle surface and volume, respectively. The size spectrum $n_p(p)$ in a given coordinate is related with $n_r(r)$ via the following relation of measures: $n_p(p)dp = n_r(r)dr$ so the total number $N = \int n_r dr$ is conserved.

Second, there is also a degree of freedom in the choice of the grid layout $p(r(x))$, that is how the parameters $r$, $s$ or $v$ are discretized to form the equidistant grid in $x$. This can be used, for instance, to define a mass-doubling grid layout ($x = \ln_2(r^3)$) as used in Morrison et al. (2018) and herein.

Combining the two transformations results in the following definition of $G$:

$$G \equiv dp(r)/dx(r) = \frac{dp}{dx} \tag{1.2}$$

which defines the transformation from the coordinate $p$ of the density function to the numerical mesh coordinate $x$. For further discussion of the coordinate transformation approaches in the embraced framework (including multi-dimensional setting), see Smolarkiewicz and Clark (1986) and Smolarkiewicz and Margolin (1993).

## 2 Spectral advection with upwind and MPDATA (box-model test case)

### 2.1 Upwind discretization

The numerical solution of equation (1.1) will be obtained by discretizing space and time as follows: $x = \mathrm{i} \cdot \Delta x$ and $t = \mathrm{n} \cdot \Delta t$. Henceforth, $\psi_\mathrm{i}^\mathrm{n}$ and $G_\mathrm{i}$ denote the discretized number density $n_p$ and the discretized coordinate transformation term, respectively. The dimensionless advective field is denoted by $GC = \frac{dp}{dx} u \Delta t / \Delta x$, where $C$ stands for the Courant number, i.e. the velocity in terms of temporal and spatial grid increments. A staggered grid is employed what warrants introduction of fractional indexing for vector fields, i.e.: $GC_{\mathrm{i}+1/2} \equiv (GC)|_{\mathrm{i}+1/2}$ in the case of the discretisation of the product $GC$. To solve the equation numerically, a finite difference form of the differential operators is introduced embracing the so-called upwind approach (dating back at least to Courant et al., 1952, eq. 16 therein):

$$\psi_\mathrm{i}^{\mathrm{n}+1} = \psi_\mathrm{i}^\mathrm{n} - \frac{1}{G_\mathrm{i}} \Big( F(\psi_\mathrm{i}^\mathrm{n}, \psi_{\mathrm{i}+1}^n, GC_{\mathrm{i}+1/2}) - F(\psi_{\mathrm{i}-1}^\mathrm{n}, \psi_\mathrm{i}^\mathrm{n}, GC_{\mathrm{i}-1/2}) \Big) \tag{2.1}$$

with

$$F(\psi_L, \psi_R, GC_\mathrm{mid}) = \max(GC_\mathrm{mid}, 0) \cdot \psi_L + \min(GC_\mathrm{mid}, 0) \cdot \psi_R \tag{2.2}$$

where the introduced flux function $F$ defines the flux of $\psi$ across grid-cell boundary as a function of the values of $\psi_L$ and $\psi_R$ to the left and right of the boundary, respectively and the value of $GC$ at the boundary. Hereinafter a shorthand notation $F_{i+\frac{1}{2}}(\psi) \equiv F(\psi_i, \psi_{i+1}, GC_{i+\frac{1}{2}})$ is used.

### 2.2 ~~Test~~ Box-model test case and upwind solution

The test case is based on Figure 3 from East (1957) - one of the early papers on the topic of cloud droplet spectral broadening. The case considers the growth of a population of cloud droplets through condensation in the equilibrium supersaturation limit, where:

$$u \approx \frac{dx}{dr}\dot{r} = \frac{dx}{dr}\frac{\xi}{r}, \tag{2.3}$$

with $\xi = \xi_0(S-1)$ being an approximately constant factor proportional to supersaturation $(S-1)$. The parameter $\xi_0$ is set to $100\ \mu\mathrm{m}^2\mathrm{s}^{-1}$ to match the results from East (1957).

For the initial number density distribution function, an idealized fair-weather cumulus droplet size spectrum is modeled with a lognormal distribution:

$$n_r^{(0)}(r) = n_0 \exp\left(-\kappa(\log_{10}(r/r_0))^2\right)/r \tag{2.4}$$

with parameters: $r_0 = 7\ \mu\mathrm{m}$, $n_0 = 465\ \mathrm{cm}^{-3}$ and $\kappa = 22$.

For the boundary conditions (implemented using halo grid cells), extrapolation is applied for $G$, while both $\psi$ and $GC$ are set to zero within the halo.

Analytical solution to eq. (1.1) is readily obtainable for $\dot{r} = \xi/r$ and for any initial size distribution. Noting that introducing $x = r^2$ coordinates, the transport equation (1.1) becomes a constant-coefficient advection equation, the problem reduces to translation of the signal in $x$ by $2\xi t$. Cast in the $r$ coordinate, the solution can be expressed as (Kovetz, 1969):

$$\psi^{\text{analytical}} = n_r(r, t > 0) \equiv \frac{r}{\tilde{r}} n_r^{(0)}(\tilde{r}), \tag{2.5}$$

where $\tilde{r} = \tilde{r}(r, t) = \sqrt{r^2 - 2\xi t}$.

The upper panels in Figures 1 and 2 depict the droplet size spectrum evolution through condensational growth from an initial liquid water mixing ratio of $M_0 = 1\ \mathrm{g\,kg^{-1}}$ under supersaturation $S - 1 = 0.075\%$.

Two grid layout ($x$) and size parameter ($p$) choices are depicted. Both panels in Fig. 1 present simulation carried out with density function coordinate $p = r^2$ and discretized on a mass-doubling grid ($x = \ln_2(r^3)$), whereas both panels in Fig. 2 present simulation results obtained with $x = r$ and $p = r$. In both cases, the timestep is set to $\Delta t = \frac{1}{3}$ s, the domain range is (1; 26) $\mu$m, there are 75 grid cells. Such settings corresponds to $GC \approx 0.26$ in first layout, where $p = r^2$ is used, and variable Courant number approximately in the range of (0.03; 0.07) in second layout, where $p = r$ is used.

The snapshots are depicted at times where the liquid water mixing ratio of the analytical solution obtains values of 1, 4 and $10\ \mathrm{g\,kg^{-1}}$ (assuming air density of $1\ \mathrm{kg\,m^{-3}}$). In both Figure 1 and 2, the upper panels display the number density and the bottom panel show the normalized mass density. The bottom panels thus depict the same quantities as Fig. 3 in East (1957).

The normalized mass density of bin $i$ is evaluated as $4/3\pi\rho_l m_i^{(l=3)}/M$ by calculating the third statistical moment of the number distribution $n_r(p)$ with the formula:

$$\begin{aligned} m_i^{(l)} &= \int_{r_1}^{r_2} n_r r^l dr = \\ &= \psi_i \cdot \begin{cases} (l+1)^{-1} r^{l+1}\Big|_{r_1}^{r_2} & \text{for } p = r \\ 2\,(l+2)^{-1} (r^2)^{\frac{l+2}{2}}\Big|_{r_1^2}^{r_2^2} & \text{for } p = r^2 \end{cases} \end{aligned} \tag{2.6}$$

where $r_1$, $r_2$ are the boundaries of $i$-th bin, and $\psi_i$ is the value of $n_p$ associated with the bin (i.e., $n_p$ is assumed to be bin-wise constant; note that the dimension of $n_p$ depends on the choice of p). The normalization factor $M$ is the mixing ratio (e.g., $M = M_0 = 1\ \mathrm{g\,kg^{-1}}$ for $t = 0$).

The dotted curve corresponds to the analytic solution. The numerical solution obtained with the upwind scheme (2.1) is plotted with red histograms and compared with the discretized analytical solution plotted as grey filled histograms.

Looking at the mass density plots in Figs. 1 and 2, it is evident that casting the results in the form of mass density shifts positions of the extrema in comparison with analytical solution. This is one of the consequences of applying numerical solution by integrating number conservation law (for discussion see sec. 2.2).

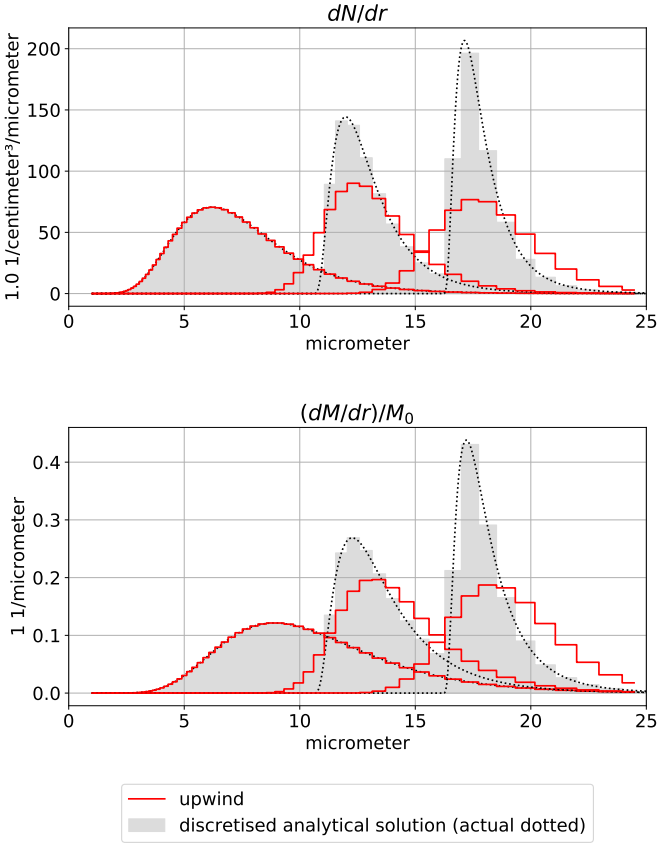


**Figure 1.** Evolution of the particle number density (upper panel) and normalized mass density (bottom panel) with red histograms corresponding to the numerical solution using upwind scheme, black dots depicting analytical solution, and gray filled histogram representing discretized analytical solution; compare Fig. 3 in East (1957). Numerical solution was obtained in the following coordinate transformation: $p = r^2$; $x = \ln_2(r^3)$

As can be seen in both the number- and mass-density plots in Figs. 1 and 2, solutions obtained with the upwind scheme are characterized by significant drop in the peak value and spectral broadening, with respect to the analytical solution – both manifesting the numerical diffusion.

The broadening and the drop in the peak value is less pronounced in Fig. 2 where the linear grid increases the resolution in the large-particle region of the spectrum.

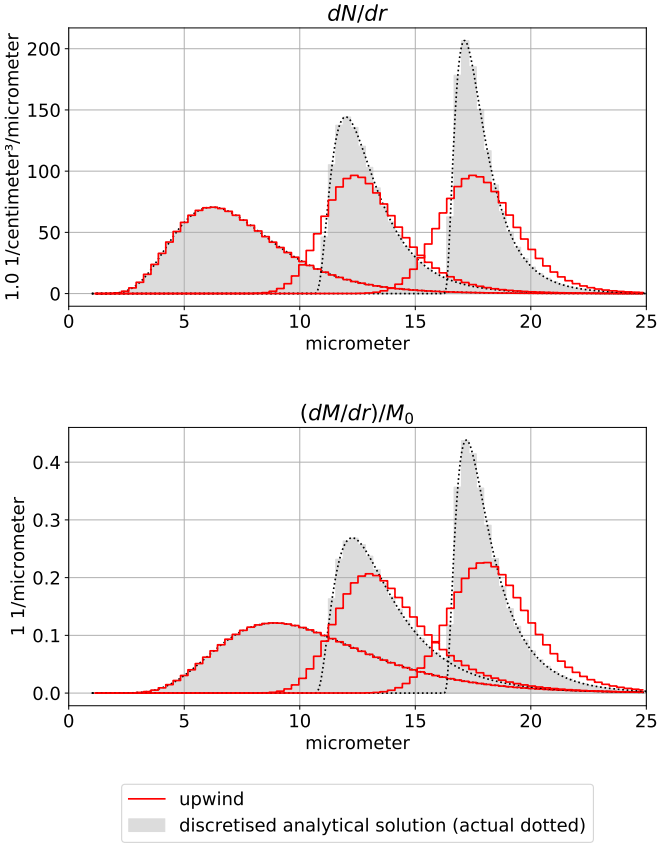


**Figure 2.** As in Fig. 1 for $p = r$ and $x = r$.

## 3 ~~MPDATA~~

### 2.1 Truncation error analysis of the upwind scheme

One of the methods used to quantify the numerical diffusion of the upwind scheme is the modified equation analysis of Hirt (1968) (see Margolin and Shashkov, 2006, for discussion in the context of MPDATA). To depict the idea, a simplified setting of $G = 1$ and $C = \text{const}$ is outlined herein. In the analysis, the Taylor expansion of $\psi$ up to the second order is taken at $\psi_i^{n+1}$, $\psi_{i+1}^n$ and $\psi_{i-1}^n$ and substituted into the numerical upwind scheme, in which the flux function (2.2) is expressed using moduli (e.g., Crowley, 1968, eq. (12)):

$$\psi_i^{n+1} = \psi_i^n - \left( \frac{C + |C|}{2} (\psi_i^n - \psi_{i-1}^n) + \frac{C - |C|}{2} (\psi_{i+1}^n - \psi_i^n) \right) \tag{2.1}$$

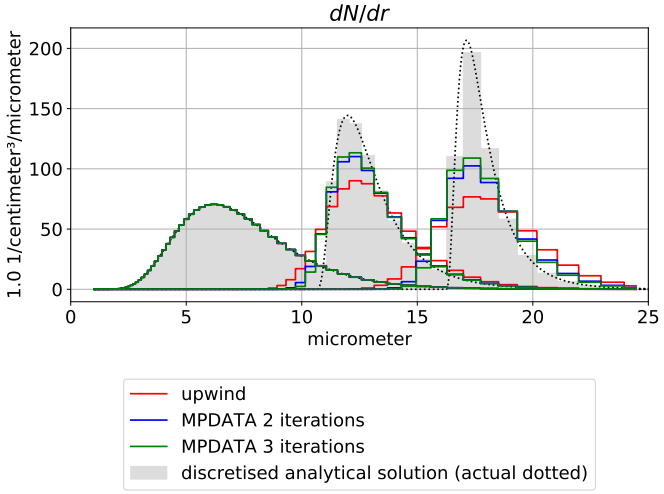


**Figure 3.** Comparison of analytic, upwind and MPDATA solutions (see plot key for algorithm variant specification) using the setup from Fig. 1, see sec. 2.2 for discussion.

resulting in:

$$\partial_t\psi + \partial_t^2\psi\frac{\Delta t}{2} = -\frac{u+|u|}{2}\left(\partial_x\psi - \partial_x^2\psi\frac{\Delta x}{2}\right) - \frac{u-|u|}{2}\left(\partial_x\psi + \partial_x^2\psi\frac{\Delta x}{2}\right) \tag{2.2}$$

which is further transformed by employing a time derivative of both sides of the original advection equation $\partial_t\psi = -u\partial_x\psi \longrightarrow \partial_t^2\psi = -u\partial_x\partial_t\psi = u^2\partial_x^2\psi$ to substitute the second-order time derivative with spatial derivative (Cauchy-Kowalevski procedure, see Toro, 1999) leading to the sought modified equation (Roberts and Weiss, 1966, eq. 2.9):

$$\partial_t\psi + u\partial_x\psi + \underbrace{\left(u^2\frac{\Delta t}{2} - |u|\frac{\Delta x}{2}\right)}_{\mathrm{K}}\partial_x^2\psi + \ldots = 0 \tag{2.3}$$

The above analysis depicts that the employment of the numerical scheme (2.1) results in a solution of a modified equation (2.3), approximating the original problem up to first order. The leading second-order error contribution has the form of a diffusive term with a coefficient $K$ (note that the above outline of the modified equation analysis assumes the constant velocity field). The diffusive form of the leading error term explains with the smoothing of the spectrum evident in Figs. 1,2, and hence the notion of numerical diffusion.

### 2.2 Antidiffusive velocity and iterative corrections

The problem of numerical diffusion can be addressed by introducing the so called “antidiffusive velocity" (Smolarkiewicz, 1983). To this end, the Fickian flux can be cast in the form of the advective flux - an approach dubbed pseudo-velocity technique

in the context of advection-diffusion simulations (Lange, 1973, 1978) or hyperbolic formulation of diffusion (Cristiani, 2015, discussion of eq. (4) therein), and discussed in detail in Smolarkiewicz and Clark (1986, sect. 3.2):

$$\partial_x(K\partial_x\psi) = \partial_x\left(K\frac{\partial_x\psi}{\psi}\psi\right). \tag{2.4}$$

In Smolarkiewicz (1983, 1984), it was proposed to apply the identity (2.4) to equation (2.3) in order to suppress the spurious diffusion. The procedure is iterative. The first iteration is the basic upwind pass. Subsequent corrective iterations reverse the effect of numerical diffusion by performing upwind passes with the so-called antidiffusive flux based on equation (2.4) but with $K$ taken with negative sign and approximated using the upwind stencil (for discussion of the discretization, see Smolarkiewicz and Margolin (2001)).

Accordingly, the basic antidiffusive field $GC^{(k)}$ is defined as follows (with $\epsilon > 0$ being an arbitrary small constant used to prevent from divisions by zero):

$$GC^{(k)}_{i+\frac{1}{2}} = A_{i+\frac{1}{2}}\left(\left|GC^{(k-1)}_{i+\frac{1}{2}}\right| - \left(GC^{(k-1)}_{i+\frac{1}{2}}\right)^2\right), \tag{2.5}$$

where $k$ is the iteration number, $GC^{(1)} \equiv GC$ and

$$A_{i+\frac{1}{2}} = \frac{\psi^*_{i+1} - \psi^*_i}{\psi^*_{i+1} + \psi^*_i + \epsilon}, \tag{2.6}$$

where $\psi^*$ denotes $\psi^n$ in the first iteration, or the values resultant from application of the upwind scheme with the antidiffusive flux in subsequent iterations. The MPDATA scheme inherits the key properties of upwind in terms of positive-definiteness, conservativeness and stability, while reducing the effect of numerical diffusion. Given the context of conservation of particle concentration, in all presented numerical formulæ below, it is assumed that the transported signal is positive, the references provided include formulation of the algorithm for variable sign signals.

Figure 3 compares a set of example simulations performed with the same set-up as in Figure 1. The analytical results obtained with upwind are supplemented with results obtained using MPDATA scheme with two and three iterations. Employment of the MPDATA iteration corrects both the signal peak amplitude and its width, as well as the position of the maximum. It is visible that the effect of the third iteration is less pronounced than that of the second one. Overall, while the MPDATA solutions are superior to upwind, the drop in amplitude and broadening of the resultant spectrum still visibly differs from the discretized analytical solution.

### 2.3 Infinite gauge variant

For the possible improvement of the algorithm, one may consider linearizing MPDATA about an arbitrarily large constant (i.e. taking $\psi' = \psi + a\chi$ in the limit $a \longrightarrow \infty$ instead of $\psi$, where $\chi$ is a constant scalar background field). Such analysis was considered in Smolarkiewicz and Clark (1986, eq. 41) and subsequently referred to as the "infinite-gauge" (or "iga") variant of MPDATA (Smolarkiewicz (2006, eq. 34), Margolin and Shashkov (2006, point (6) on page 1204)).

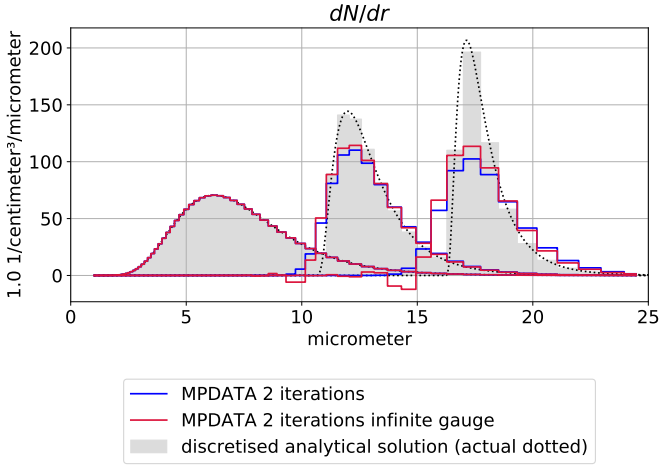


**Figure 4.** Comparison of analytic, upwind and MPDATA solutions (see plot key for algorithm variant specification) using the setup from Fig. 1, see sec. 2.3 for discussion.

Such gauge transformation changes the corrective iterations of the basic algorithm as follows (replacing eqs. (2.6) and (2.2) what is symbolized with $\rightsquigarrow$):

$$A_{i+\frac{1}{2}} \quad \rightsquigarrow \quad A^{(\text{iga})}_{i+\frac{1}{2}} = \frac{\psi^*_{i+1} - \psi^*_i}{2} \tag{2.7}$$

$$F_{i+\frac{1}{2}} \quad \rightsquigarrow \quad F^{(\text{iga})}_{i+\frac{1}{2}} = GC^{(k)}_{i+\frac{1}{2}} \tag{2.8}$$

Noting that the amplitude of the diffusive flux (2.4) is inversely proportional to the amplitude of the signal, such gauge choice decreases the amplitude of the truncation error (see Smolarkiewicz and Clark (1986, p. 408), Jaruga et al. (2015, discussion of Fig. 11)), however it makes the algorithm no longer positive definite.

Figure 4 depicts how enabling the infinite gauge variant influences results presented in Figure 3. In each plotted ~~time step~~timestep, the maximum amplitude of the infinite-gauge result is closest to the analytical solution improving over the basic MPDATA. However, in each case negative values are observed (non-physical in case of the considered problem).

Consequently, for the problem at hand, it is effectively essential to combine it with the monotonicity-preserving non-oscillatory option outlined in the next section.

## 2.4 Non-oscillatory option

In Smolarkiewicz and Grabowski (1990), extension of the MPDATA algorithm was introduced that makes the solution monotonicity preserving and precludes appearance of negative values in the discussed solution of droplet size spectrum evolution. The trade-off is that the order of the algorithm is reduced (see Appendix A).

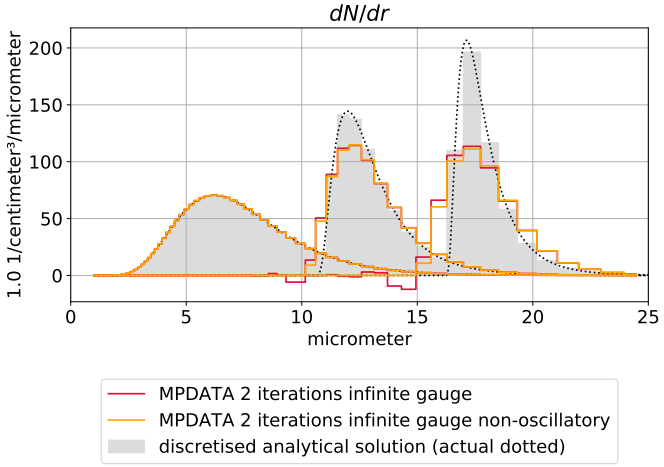


**Figure 5.** Comparison of analytic, upwind and MPDATA solutions (see plot key for algorithm variant specification) using the setup from Fig. 1, see sec. 2.4 for discussion.

The non-oscillatory option (later referred to as “non-osc" herein) modifies the algorithm in such way:

$$GC_{i+\frac{1}{2}}^{(k+1)} \rightsquigarrow GC_{i+\frac{1}{2}}^{(k+1,\text{non-osc})} = GC_{i+\frac{1}{2}}^{(k)} \times \times \begin{cases} \min(1, \beta_i^{\downarrow}, \beta_{i+1}^{\uparrow}) & GC_{i+\frac{1}{2}}^{(k)} \geq 0 \\ \min(1, \beta_i^{\uparrow}, \beta_{i+1}^{\downarrow}) & GC_{i+\frac{1}{2}}^{(k)} < 0 \end{cases}, \tag{2.9}$$

where

$$\beta_i^{\uparrow} \equiv G_i \times \frac{\max\left(\psi_i^{(\max)}, \psi_{i-1}^{*}, \psi_i^{*}, \psi_{i+1}^{*}\right) - \psi_i^{*}}{\max\left(F(\psi^*)_{i-\frac{1}{2}}, 0\right) - \min\left(F(\psi_i^*)_{i+\frac{1}{2}}, 0\right) + \epsilon}, \tag{2.10}$$

and

$$\beta_i^{\downarrow} \equiv G_i \times \frac{\min\left(\psi_i^{(\min)}, \psi_{i-1}^{*}, \psi_i^{*}, \psi_{i+1}^{*}\right) - \psi_i^{*}}{\max\left(F(\psi_i^*)_{i+\frac{1}{2}}, 0\right) - \min\left(F(\psi_i^*)_{i-\frac{1}{2}}, 0\right) + \epsilon}, \tag{2.11}$$

with

$$\psi_i^{(\min)} = \min(\psi_{i-1}^n, \psi_i^n, \psi_{i+1}^n), \tag{2.12}$$

$$\psi_i^{(\max)} = \max(\psi_{i-1}^n, \psi_i^n, \psi_{i+1}^n). \tag{2.13}$$

Note that in the case of infinite gauge option enabled, $F$ function takes form presented in eq. (2.7) (see also Hill, 2011, sect. 2.5).

Figure 5 juxtaposes infinite gauge solutions for non-oscillatory option switched on or off. The effectiveness of the latter variant is apparent as spurious negative values no longer occur.

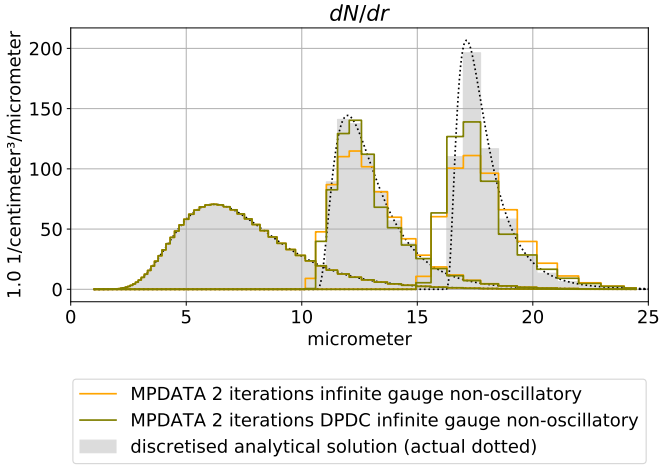


**Figure 6.** Comparison of analytic, upwind and MPDATA solutions (see plot key for algorithm variant specification) using the setup from Fig. 1, see sec. 2.5 for discussion.

### 2.5 DPDC

An alternative approach to the iterative procedure was introduced in Beason and Margolin (1988); Margolin and Smolarkiewicz (1998) and further discussed in Margolin and Shashkov (2006), where the contributions of multiple corrective iterations of MPDATA were analytically summed leading to a new two-pass scheme dubbed DPDC (double-pass donor cell), featuring the following form of the antidiffusive $GC$ field:

$$GC^{(2)}_{i+\frac{1}{2}} \rightsquigarrow GC^{(\mathrm{DPDC})}_{i+\frac{1}{2}} = \frac{GC^{(2)}}{1-|A_{i+\frac{1}{2}}|}\left(1-\frac{GC^{(2)}}{1-A^2_{i+\frac{1}{2}}}\right), \tag{2.14}$$

with $A_{i+\frac{1}{2}}$ defined in eq. (2.6). Note that only one corrective iteration is performed with the DPDC variant.

As in the case of the infinite gauge variant of MPDATA (section 2.3), the above formulation does not guarantee monotonicity of the solution. Herein an example simulation combining the DPDC, the non-oscillatory and infinite-gauge variants is presented in Figure 6 depicting how the solution is improved over that in Figure 5.

### 2.6 Divergent-flow correction

For divergent flow (hereinafter abbreviated dfl), modified equation analysis yields an additional correction term to the antidiffusive velocity (see Smolarkiewicz (1984, eq. (38)) for uniform coordinates, Margolin and Smolarkiewicz (1998, eq. (30)) for non-uniform coordinates and Waruszewski et al. (2018, sect. 4) for the infinite-gauge variant):

$$GC^{(k)}_{i+\frac{1}{2}} \rightsquigarrow GC^{(\mathrm{k,dfl})}_{i+\frac{1}{2}} = GC^{(k)} - \frac{GC^{(k)}_{i+\frac{1}{2}}}{G_{i+1}+G_i} \times \\ \times \frac{GC^{(k)}_{i+\frac{3}{2}} - GC^{(k)}_{i-1/2}}{2} \times \\ \times \begin{cases} (\psi^*_{i+1}+\psi^*_i)/2 & (iga) \\ 1 & (else) \end{cases} \tag{2.15}$$

As pointed out in section 5.1 in Smolarkiewicz (1984), this option has the potential of improving results for the problem of the evolution of the droplet size distribution (personal communication with William Hall cited therein). This is due to the drop growth velocity defined by eq. (2.3) being dependent on radius (hence divergent given the one-dimensional problem). Yet, applying adequate coordinate transformation (i.e., $p = r^2$), the drop growth velocity in the transformed coordinates becomes constant (see section 2.2 above and Hall (see, e.g. 1980, sec. 3b)). However, in simulations using the presented setup (for $p \neq r^2$; not shown), only insignificant changes in the signal occurring when the divergent-flow option was used were observed. However, the problem considered herein does not include, for instance, the surface tension influence on the drop growth rate.

### 2.7 Third order terms

Another possible improvement to the algorithm comes from the inclusion of the third-order terms in the modified equation analysis, which leads to following form of the antidiffusive velocity (Margolin and Smolarkiewicz, 1998):

$$GC^{(k)}_{i+\frac{1}{2}} \rightsquigarrow GC^{(k,\mathrm{tot})}_{i+\frac{1}{2}} = GC^{(k)} + B_i \cdot GC^{(k)}_{i+\frac{1}{2}} \times \\ \times \frac{1}{6}\left(4\frac{|GC^{(k)}_{i+\frac{1}{2}}|}{G_{i+1}+G_i} - 8\left(\frac{GC^{(k)}_{i+\frac{1}{2}}}{G_{i+1}+G_i}\right)^2 - 1\right) \tag{2.16}$$

$$B_i = 2 \cdot (\psi^*_{i+2} - \psi^*_{i+1} - \psi^*_i + \psi^*_{i-1}) \times \\ \times \begin{cases} (1+1+1+1)^{-1} & (iga) \\ (\psi^*_{i+2}+\psi^*_{i+1}+\psi^*_i+\psi^*_{i-1})^{-1} & (else) \end{cases} \tag{2.17}$$

Figure 7 depicts how enabling the third-order-terms improves solution of the test problem with respect to the upwind and basic MPDATA.

Noteworthy, discussion of higher-order variants of MPDATA was carried forward in Kuo et al. (1999) and Waruszewski et al. (2018). In the latter case, the focus was placed on accounting for coordinate transformation and variable velocity in the derivation of antidiffusive velocities leading to a fully third-order accurate scheme.

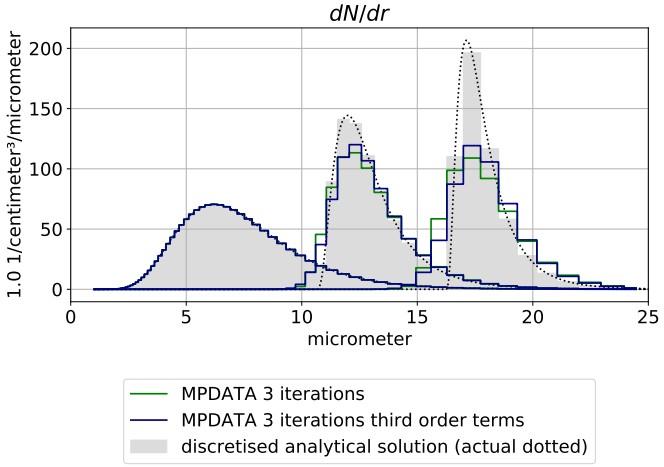


**Figure 7.** Comparison of analytic, upwind and MPDATA solutions (see plot key for algorithm variant specification) using the setup from Fig. 1, see sec. 2.7 for discussion.

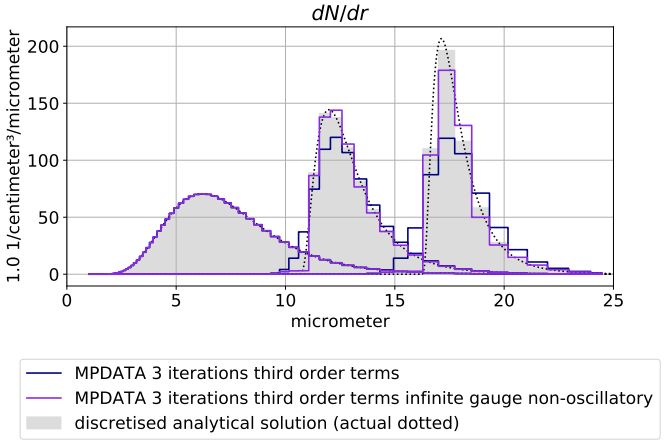


**Figure 8.** Comparison of analytic, upwind and MPDATA solutions (see plot key for algorithm variant specification) using the setup from Fig. 1, see sec. 2.8 for discussion.

### 2.8 A "best" combination of options

The MPDATA variants presented in the preceding sections can be combined together. In Figure 8, results obtained with upwind scheme and the basic two-pass MPDATA are compared with those obtained with a powerful combination of three iterations, third-order-terms, infinite-gauge and non-oscillatory options hereinafter referred to as the "best" variant (for the problem at hand).

**Table 1.** Relative dispersion of the discretized (using grid setup as in Fig. 1) analytical solution taken for five selected times.

| Variant | $d_{\text{analytic}}$ |
|---|---|
| $d(M = 1\ \text{g kg}^{-1})$ | 0.357 |
| $d(M = 2\ \text{g kg}^{-1})$ | 0.202 |
| $d(M = 4\ \text{g kg}^{-1})$ | 0.126 |
| $d(M = 6\ \text{g kg}^{-1})$ | 0.097 |
| $d(M = 8\ \text{g kg}^{-1})$ | 0.080 |
| $d(M = 10\ \text{g kg}^{-1})$ | 0.069 |

## 3 ~~Results and discussion~~

In the following subsections, the influence of MPDATA algorithm variant choice on the resultant spectrum broadness and computational cost is analysed using the example simulation setup used above (i.e., in all figures except Fig. 2, see section 2.2 for test case definition).

Analysis of the scheme solution convergence with changing resolution and Courant number is presented in Appendix A.

### 2.1 Quantification of numerical broadening

The relative dispersion, defined as the ratio of standard deviation $\sigma$ to the mean $\mu$ of the distribution, is a parameter commonly used to describe the width of the spectrum (e.g. Chandrakar et al., 2018).

The calculated dispersion ratio over all bins takes form:

$$d = \frac{\sqrt{\frac{1}{N}\sum_i m_i^{(l=2)} - \left(\frac{1}{N}\sum_i m_i^{(l=1)}\right)^2}}{\frac{1}{N}\sum_i m_i^{(l=1)}} \tag{2.1}$$

where $m_i$ is defined in (2.6) and $N$ is the conserved total number of particles (equal to $\sum_i m_i^{(l=0)}$). To quantify the effect of numerical diffusion on the broadness of the resultant spectrum, the following parameter is introduced based on the numerical and analytical solutions (hereinafter reported in percentages):

$$R_{\text{disp}} = d_{\text{numerical}}/d_{\text{analytical}} - 1 \tag{2.2}$$

Table 1 depicts the gradual narrowing of the spectrum under undisturbed adiabatic growth.

Left panel in Fig. 9 provides values of the ~~$R_{\text{disp}}$~~ $R_{\text{d}}$ parameter evaluated at six selected timesteps corresponding to $M = 1, 2, 4, 6, 8, 10\ \text{g kg}^{-1}$. Although numerical broadening is inherent to all employed schemes, and grows in time for all considered variants, the scale of the effect is significantly reduced when using MPDATA.

In particular, a tenfold decrease in numerical broadening as quantified using ~~$R_{\text{disp}}$~~ $R_{\text{d}}$ is observed comparing upwind and "best" variant considered herein.

While outside of the scope of the present study, it is worth noting that in simulations combining spectral growth with transport in physical space, the numerical broadening associated with the spatial advection also contributes to the numerical broadening effect (see Hernandéz Pardo et al., 2020, and references therein).

### 2.2 Notes on conservativeness

Due to the formulation of the problem as number conservation and discretization of the evolution equation using fixed bins, even though the numerical scheme is conservative (up to subtle limitations outlined below), evaluation of other statistical moments of the evolved distribution from the number density introduces an inherent discrepancy from the analytical results (for a discussion on multi-moment formulation of the problem, see e.g. Liu et al., 1997).

In order to quantify the discrepancy in the total mass between the discretized analytical solution and the numerically integrated spectrum, the following ratio is defined using moment evaluation formula (2.6):

$$R_M = M^{(\text{numeric})}/M^{(\text{analytic})} - 1 = \\ = \frac{\sum_i m_i^{(l=3,\ \text{numeric})}}{\sum_i m_i^{(l=3,\ \text{analytic})}} - 1. \tag{2.3}$$

Right panel in Fig. 9 depicts the values of the above-defined ratio computed for spectra obtained with different variants of MPDATA discussed herein. The departures from analytically-derived values are largest for the upwind scheme (up to ca. 5%), and oscillate around 0 with amplitude of the order of 1% for most of the MPDATA solutions.

The consequences of mass conservation inaccuracies in the fixed-bin particle size spectrum representation may not be as severe as in, e.g. dynamical core responsible for transport of conserved scalar fields. The outlined discrepancies may be dealt with by calculating the change in mass during a ~~time step~~ timestep from condensation, then using it in vapor and latent heat budget calculations so the total mass and energy in the modeled system are conserved.

The problem embodied in equation (1.1) is the conservation of number of particles and the embraced algorithm (2.1)-(2.2) is conservative (up to numerical precision) for $G = 1$. However, the formulation of the donor cell scheme $\psi^{n+1} = \psi^n + G_i^{-1}\left(F_{i-1/2} + F_{i+\frac{1}{2}}\right)$ on the staggered grid with $G \neq 1$, for example due to employment of non-identity coordinate transformations implies that even though the influx and outflux across boundary of adjacent cells is equal, discretization of $G_i$ at cell centers limits the level of accuracy in number conservation.

The total number of particles in the system may diverge from the analytical expected value even for the initial condition depending on the employed discretization approach. In the present work, the probability density function is probed at cell centers effectively assuming piecewise-constant number density function. An alternative approach is to discretise the initial probabilities by assigning to $\psi_i$ the values of $(\phi_{i+\frac{1}{2}} - \phi_{i-1/2})/(r_{i+\frac{1}{2}} - r_{i-1/2})$ where $\phi$ is the cumulative distribution.

### 2.3 Computational cost

Table 2 includes an assessment of the relative computational cost of the explored variants of MPDATA. The performance was estimated by repeated measurements of the wall time and selecting the minimal value as representative. Values are reported

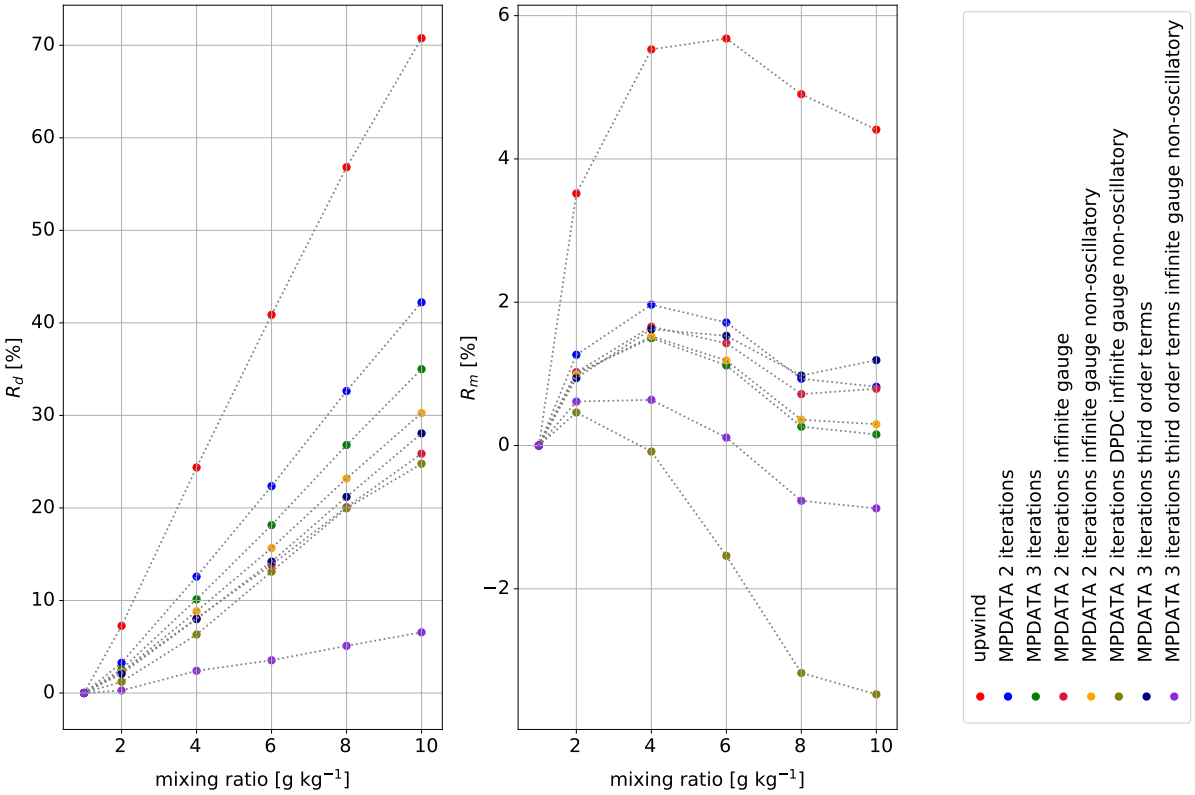


**Figure 9.** Left panel summarizes values of ~~$R_d$ (see eq.~~ the numerical-to-analytical spectral width ratio $R_\mathrm{d} = d_\mathrm{numerical}/d_\mathrm{analytical} - 1$ ~~(2.2) for definition~~expressed as a percentage) computed for simulations using different discussed variants of MPDATA and plotted as a function of increasing mixing ratio (i.e., each simulation is depicted with a set of line-connected points corresponding to selected timesteps), see section 2.1. Right panel presents analogous analysis for $R_m$, see section 2.2 for discussion. Note: $R_M = R_d = 0$ corresponds to perfect match with the analytical solution.)

after normalization with respect to the values pertinent to upwind runs. The "best" variant is roughly ten times more costly than the upwind scheme. The table includes analogous measurements reported in earlier studies on MPDATA, where available (see Table caption for comments).

As can be seen from the table, the infinite gauge option not only improves result, but simplifies equation, making numerics faster. Three-pass MPDATA with third order terms included is slightly faster than the variant with both the infinite-gauge and non-oscillatory options enabled.

Although the discussed problem is one-dimensional, its computationally efficient and accurate solution is essential, as it typically needs to be solved at every ~~time step~~ timestep and grid point of a three-dimensional cloud model.

**Table 2.** Elapsed wall times with respect to upwind computed for mass doubling grid for results presented herein compared with with data reported in three previously published works. Column labeled with S83 denotes values reported in Smolarkiewicz (1983) for two-dimensional problem. Column labeled SS05 correspond to data reported in Smolarkiewicz and Szmelter (2005) for a 3D finite-volume advection on unstructured grid. Column SR91 includes values from Smolarkiewicz and Rasch (1991), MSS00 corresponds to data from Margolin et al. (2000), both reported for two-dimensional problems.

| Variant | | S83 | SS05 | SR91 | MSS00 |
|---|---|---|---|---|---|
| upwind | 1.0 | 1.0 | 1.0 | 1.0 | 1.0 |
| 2 pass | 2.5 | 2.9 | 4.3 | 5.4 | 3.7 |
| 2 pass, iga | 2.2 | - | 1.9 | - | - |
| 2 pass, iga, non-osc | 5.9 | - | 3.9 | - | - |
| DPDC, iga, non-osc | 6.2 | - | - | - | - |
| 3 pass | 5.7 | 5 | - | 9.8 | - |
| 3 pass, tot | 4.1 | - | - | 19 | - |
| 3 pass, tot, iga, non-osc | 11 | - | - | - | - |

# 3 Spectral-spatial advection with MPDATA (single-column test case)

## 3.1 Problem statement

In multidimensional simulations in which the considered particle number density field is not only a function of time and of particle size, but also of spatial coordinates, there are several additional points to consider applying MPDATA to the problem.

First, in the context of atmospheric cloud simulations, owing to the stratification of the atmosphere, a usual practice is to reformulate the conservation problem in terms of specific number concentration being defined as the number of particles $n_p$ (cf. eq. (1.1)) divided by the mass of air (commonly the dry air) effectively resulting in multiplication of the $G$ factor (cf. eqs (1.2)-(2.1)) by the (dry) air density. This translates to maintaining a constant specific number concentration (summed across all particle size categories) along the vertical dimension despite presence of an air density gradient. Ordinary particle volume concentration would vary due to variable density of air (i.e., expansion of air along the vertical coordinate). Note however, that in eq. (2.1) it is assumed that the $G$ factor does not vary in time.

Second, even with a single spatial dimension (single-column setup), the coupled size-spectral/spatial advection problem is two-dimensional. This is where the inherent multidimensionality of MPDATA (also, the "M" in MPDATA) requires further attention. The one-dimensional antidiffusive formulæ discussed in sections 2.2-2.7 need to be augmented with additional terms representing cross-dimensional contributions to the numerical diffusion. For introduction, see e.g. Section 2.2 in Margolin and Smolarkiewi , for original derivation see Smolarkiewicz (1984), for a recent work discussing the interpretation of all terms in the antidiffusive velocity formulæ, including cross-dimensional terms, see Waruszewski et al. (2018).

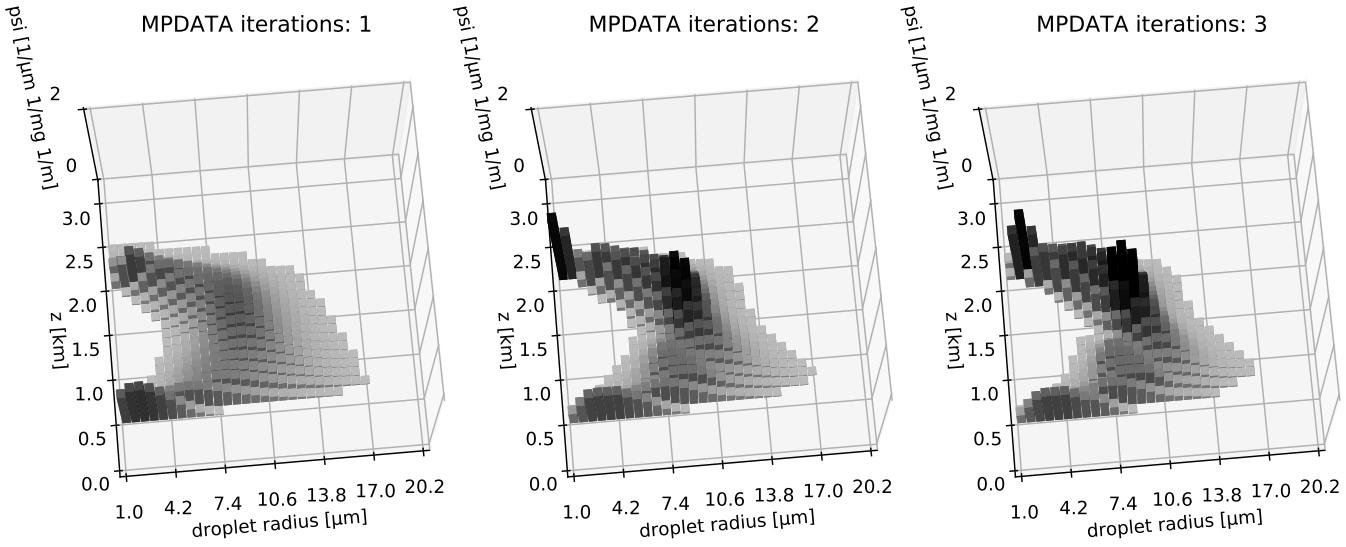


**Figure 10.** Snapshots of the advected two-dimensional liquid water field at $t = t_1 = 600$s for three different number of iterations settings of MPDATA (with the non-oscillatory option enabled).

Third, in any practical application where the drop size evolution is coupled with water vapour budget (and hence with supersaturation evolution), it is essential to evaluate the total change in mass of liquid water due to condensation which is then to be used to define the source term of the water vapour field (and in latent heat budget representation). Noteworthy, knowing the difference of values at n + 1 and at n timesteps of the advected specific number concentration field is not sufficient to evaluate the vapour sink/source term. This is because only the fluxes across the size-spectral dimension need to be accounted for (note that the fluxes in all MPDATA iterations need to be summed up).

There are several recent papers highlighting the need for scrutiny when comes to the interplay of size-spectral and spatial advection and the associated numerical broadening (Morrison et al., 2018; Hernandéz Pardo et al., 2020; Lee et al., 2021). In the following subsection, a set of single-column simulations is presented and discussed depicting performance of MPDATA in a size-spectral/spatial advection problem coupled with vapour advection and supersaturation budget. The simulations are performed using a commonly employed MPDATA setting with only the non-oscillatory option enabled, and the discussion is focused on the sensitivity of the results to spatial, spectral and temporal resolution, as well as to the effect of performing one or two corrective passes of MPDATA (two or three iterations, respectively).

### 3.2 Test case definition

The test setup is based on the single-column KiD warm case introduced in Shipway and Hill (2012). This prescribed-flow framework has been further used, e.g., in Field et al. (2012) (mixed-phase scenario), in Hill et al. (2015) (warm rain scenario) and in Gettelman and Morrison (2015) (both pure-ice, mixed-phase and warm-rain scenarios). Here, condensation is the only microphysical process considered.

The simulated 3.2 km height column of air is described by: a constant-in-time piecewise-linear potential temperature profile (297.9 K from the ground to the level of 740 m, linearly decreasing down to 312.66 K at 3260 m); constant-in-time hydrostatic pressure and density profiles computed assuming surface pressure of 1007 hPa; piece-wise linear initial vapour mixing ratio profile (15 $\mathrm{g\,kg^{-1}}$ at ground, 13.8 $\mathrm{g\,kg^{-1}}$ at 740 m and 2.4 $\mathrm{g\,kg^{-1}}$ at 3260 m); and a constant-in-space but time-dependent vertical momentum defined by $\rho_d w(z,t) = \rho_d w_1 \sin(\pi t/t_1)(1 - H(t - t_1))$ where $H$ is the Heaviside step function, $w$ is the vertical velocity, $w_1 = 2.5$ $\mathrm{m\,s^{-1}}$, $\rho_d$ is the hydrostatic dry density profile and $t_1 = 600$ s. Note that the vertical velocity thus differs from the original KiD setup where $w$ is held constant, the change is motivated by the aim of maintaining the non-divergent flow field condition.

The advection is thus solved for two scalar fields: (i) a one-dimensional field representing vertical variability of water vapour mixing ratio (mass of vapour per mass of dry air) and (ii) a two-dimensional field representing vertical and spectral variability of liquid particle specific concentration (number of particles per mass of dry air). The spectral coordinate is set to particle radius ($p = r$) and the bins are laid out uniformly ($x = r$) over a range of 1 $\mu$m to 20.2 $\mu$m. Noteworthy, this results in the size-spectral component of the advection velocity being divergent (while the vertical component is non-divergent).

The initial condition does not feature supersaturation anywhere in the domain. The upward advection of water vapour causes supersaturation to occur and trigger condensation. The size-spectral velocity is defined as in the box-model test case (cf. eq. (2.3)) but with supersaturation being time-dependent and derived from the values of vapour mixing ratio, temperature and pressure at a given level. Note that the temperature profile is constant in time and the test case does not feature representation of latent heat release effects, only the ambient air/particle vapour budget is accounted for by subtracting the amount of condensed water from the vapour field in each timestep, prior to performing subsequent step of advetion on the vapour mixing ratio field.

The domain is initially void of liquid water and the only source of it is through the boundary condition in the spectral dimension specified as follows:

$$\psi_{-1} = \max\left(0, N_{\mathrm{CCN}} - \sum_i \psi\right) \tag{3.1}$$

with $i = -1$ denoting the halo grid cell at the left edge of the spectral domain on a given vertical level and the summation spans all bins at a given level (excluding halo grid cells). The flux across the domain boundary in the spectral dimension represents cloud droplet activation. The flux is dependent, through eq. (2.3) on the supersaturation at a given level, and on the $N_{\mathrm{CCN}}$ parameter representing a maximal number of activated droplets (per unit mass of dry air). In the performed simulations, $N_{\mathrm{CCN}}$ was set to 500 $\mathrm{mg^{-1}}$. For discussion of other ways to represent activation in bin microphysics models, see, e.g., Grabowski et al. (2011).

The simulations are run for 15 minutes out of which the first 10 involve non-zero vertical velocity (as $t_1 = 600$ s).

### 3.3 Discussion of results

Figure 10 depicts qualitatively how MPDATA performs with the single-column simulation depending on the number of MPDATA iterations employed. Presented simulation, hereinafter referred to as base resolution case, is performed with the liquid water dynamics resolved on a $32 \times 32$ grid with vertical grid step $\Delta z = 100$ m, size-spectral grid step $\Delta r = 0.6$ $\mu$m and timestep $\Delta t = 0.25$s. The two-dimensional liquid water mixing ratio grid is rendered with shaded array of histogram bars. The vertical axis corresponds to the advected quantity: spatio-spectral number density divided by the dry density of air. Histogram bars with value of less than 1% of the vertical axis range ($1\% \times 2$ m$^{-1}$mg$^{-1}$$\mu$m$^{-1}$) are not plotted for clarity. Presented plots are aimed at intuitively portraying the model state and the extent to which introduction of subsequent MPDATA corrective iterations counteracts the numerical spectrum broadening. Note that besides the depicted liquid water mixing ratio, the model state consists as well of a one-dimensional vapour mixing ratio vector.

In Figure 11, the base resolution case is depicted with plots constructed following the original methodology from Shipway and Hill (2012) (as in Fig. 1 therein). The gray-scale maps depict the evolution in time and vertical dimension of: water vapour mixing ratio $q_l$, supersaturation $S$ and the droplet spectrum relative dispersion $d$. The adjacent profile plots depict the vertical variability of the mapped quantity at four selected times.

Notwithstanding the highly idealised and simplified modeling framework employed herein, one may attempt comparison with profiles obtained from both in-situ aircraft measurements (Arabas et al., 2009, profiles of $d$ in Fig. 1 therein) and detailed three-dimensional simulations (Arabas and Shima, 2013, profiles of $S$ and liquid water content in Fig. 2-4 therein) inspired by the same RICO field campaign (Rauber et al., 2007) as the single-column setup of Shipway and Hill (2012). The resemblance remains qualitative, as expected given the stark simplicity of the KiD framework, yet it is arguably congruous enough to confirm that the chosen test case covers the parameter space relevant to the studied problem.

The liquid water profiles depicted in the top row of Fig. 11 reveal that the cloud structure developed within the first ca. 9 minutes of the simulation is later maintained, with the profiles at $t = 9$ min. and $t = 12$ min. being virtually indistinguishable. Middle row plots of supersaturation profiles depict that the considered simulation setup enables to capture the characteristic supersaturation maximum just above cloud base. Furthermore, it is evident that the corrective iterations of MPDATA influence the maximal supersaturation values. Noteworthy, this results in different timestep (Courant number) constraints depending on the number of iterations used because the spectral velocity is a function of supersaturation. The bottom row in Fig. 11 depicts the relative dispersion defined and computed as in section 2.1, discarding levels where the total droplet number mixing ratio summed over all bins on a level is below 5% of $N_{\mathrm{CCN}}$. Narrowing of the spectrum with height below $z = 1.5$ km depicted by decreasing values of $d$ is a robust feature. Minimal values of $d$ vary visibly depending on the number of MPDATA iterations employed.

In order to provide insight into the sensitivity of the results to temporal, spatial and spectral resolution, Fig. 12 presents the relative dispersion profiles at $t = t_1 = 10$ min. for several resolution settings. In the background of the figure, there are three axes plotted pointing the directions in which the figure panels can be explored to reveal the dependence on: the vertical spatial spacing $\Delta z$ (left-to-right), the spectral spacing $\Delta r$ (bottom-to-top), and the timestep (back-to-foreground). The base resolution case is plotted at the intersection of the background axes. Note that besides the back-to-foreground sequence of plots where all but the timestep settings is kept equal, the timestep also varies with the grid settings to fulfill scheme stability constraints.

The dependence on the temporal resolution, as gauged by comparing the base resolution case with cases with the timestep halved ($\Delta t = 125$ ms; background) and doubled ($\Delta t = 500$ s; foreground), is barely observable. This is in general agreement with Morrison et al. (2018) and Hernandéz Pardo et al. (2020) where the dependence on timestep is shown to be much smaller than on the spatial or spectral resolution.

The dependence on spectral resolution is captured and clearly manifested at the lowest spectral resolution where the minimal spectral dispersion $d$ drops by ca. 0.1 when decreasing $\Delta r = 1.2\mu$m down to $\Delta r = 0.3\mu$m. Little further change can be observed by refining the resolution down to $\Delta r = 0.15\mu$m. Focusing on the minimal values of $d$ for a given profile, in general the lower the spectral resolution, the more profound the effect of introducing corrective iterations of MPDATA. In most cases, applying even a single corrective step (i.e., 2 iterations) results in halving of the minimal values $d$ as compared to upwind solution (i.e., 1 iteration).

The spatial resolution setting $\Delta z$ significantly alters the results particularly near cloud base. The values of $d$ at the lower half of the presented profile (i.e., ca. below $z = 1$ km) drop from over 0.3 down to around 0.1 when refining the resolution from $\Delta z = 200$ m down to $\Delta z = 25$ m.

## 4 Conclusions

The study was focused on the MPDATA family of numerical schemes that iteratively apply the upwind algorithm reducing the numerical diffusion while maintaining the salient features of the underlying upwind scheme such as conservativeness and positive-definiteness.

Several options introduced to MPDATA following its original formulation were explored here in the context of condensational growth problems. This included the procedure to introduce coordinate transformations (e.g., to a mass-doubling grid) and the variants of MPDATA including: infinite-gauge, non-oscillatory, DPDC and third-order-terms options.

Furthermore, an example application of the MPDATA scheme to address the two-dimensional advection problem arising from consideration of size-spectral/spatial evolution of the particle density in a single-column model was presented. The developed setup constitutes a Python reimplementation of the condensation-only bin-microphysics single-column variant of the KiD framework introduced in Shipway and Hill (2012). The simulations feature coupling between droplet growth and supersaturation evolution. Furthermore, the multidimensional character of MPDATA stemming from involvement of cross-dimensional terms in antidiffusive velocity formulæ is exploited. Presented analysis is focused on the sensitivity to spatial, spectral and temporal resolution and hints that, for the case considered, the cloud droplet spectrum relative dispersion is significantly influenced by numerical diffusion pertinent to both spectral and vertical advection. Focusing on the levels corresponding to the region of maximal liquid water content (ca. between $z = 1$ km and 2 km), it is evident that application of even a single MPDATA corrective iteration robustly reduces (in most cases more than halves) the spectral width. In agreement with conclusions drawn from single-column simulations in Morrison et al. (2018) and Lee et al. (2021), within the range of explored grid settings, the vertical resolution has most profound effect on the overall characteristics of the spectrum width profile as it significantly influences the just-above-cloud-base evolution of the spectral width (much less influence above).

In literature, the derivation and discussion of MPDATA variants is spread across numerous research papers published across almost four decades, and in most cases focused on multidimensional hydrodynamics applications. It ~~seems that this contributed to an apparent detachment of condensational-growth applications from the benefits of continuous research on MPDATA. It~~ was the aim of this study, to highlight the developments that followed the original formulation of the algorithm, and to highlight their applicability to the problem. To this end, it was shown that combination of such features of MPDATA as the infinite-gauge, non-oscillatory and third-order-terms options, together with application of multiple corrective iterations offer a robust scheme that grossly outperforms the almost quadragenarian basic MPDATA.

This study outlined the applicability of the PyMPDATA high-performance Python implementation of MPDATA for exploring the numerical aspects of the representation of condensational growth in bin microphysics schemes. Extensibility of PyMPDATA, in particular towards support for higher-dimensional problems, was among the key motivating factors for development of the package in Python/Numba. This opens up the path to higher-dimensional MPDATA solvers – a development already underway. A four-dimensional MPDATA solver (to the authors' knowledge not publicly released or discussed in literature yet) would be capable of integrating the bin micrphysics dynamics in three spatial dimensions.

*Code availability.* All of presented figures and tables can be recreated in interactive notebooks "in the cloud" using the mybinder.org or Colab platforms. To launch the notebooks, follow the links: https://github.com/atmos-cloud-sim-uj/PyMPDATA-examples/tree/main/PyMPDATA_examples/Olesik_et_al_2020 and https://github.com/atmos-cloud-sim-uj/PyMPDATA-examples/tree/main/PyMPDATA_examples/Shipway_and_Hill_2012.

The calculations are performed using newly developed open-source Pythonic implementation of MPDATA: PyMPDATA (Arabas et al., 2020). In terms of numerics, implementation of PyMPDATA closely follows libmpdata++ (Jaruga et al., 2015). PyMPDATA development is hosted at: https://github.com/atmos-cloud-sim-uj/PyMPDATA. PyMPDATA is licenced under the GNU General Public License 3.0.

The single-column framework is a Python reimplementation of the open-source KiD code available at https://github.com/BShipway/KiD.

## Appendix A: Convergence analysis

To assess the spatial and temporal convergence of the numerical solutions presented above, a convergence test originating from Smolarkiewicz and Grabowski (1990) is used. For the analysis the following truncation-error $L^2$ measure is used (e.g., Smolarkiewicz, 1984):

$$\mathrm{Err}_{L2} = \frac{1}{T}\sqrt{\sum_i \left(\psi_i^{\text{numerical}} - \psi_i^{\text{analytical}}\right)^2}/nx. \tag{A1}$$

As a side note, it is worth pointing out that for the chosen coordinates $\left(p = r^2, x = r^2\right)$, the coordinate transformation term is equal to identity, so there is no need for including the $G$ factor into the computed error measures. In general case, convergence

will depend on the grid choice and to account for that one may used a modified measure as given in Smolarkiewicz and Rasch (1991, eq. 24 ).

To explore the convergence, the error measures are computed for 7 different linearly spaced values of $C$ between $0.05$ and ~~.95~~$0.95$, and $nx \in \{2^7, 2^8, 2^9, 2^{10}, 2^{11}, 2^{12}, 2^{13}, 2^{14}\}$ resulting in 56 simulations for each presented combination of options.

As proposed in Smolarkiewicz and Grabowski (1990), visualization of the results is carried out on polar plots with radius $\rho$ and angle $\phi$ coordinates defined as follows:

$$\rho = \ln_2\left(\frac{1}{nx}\right) + \text{const}, \quad \phi = C\frac{\pi}{2}, \tag{A2}$$

where $\rho$ was shifted by a constant so that the highest resolution grid corresponds to $\rho = 1$.

Figures A1-A8 depict the convergence rates and are intended for comparison with analogously constructed plots in Figs. 2-3 Smolarkiewicz and Grabowski (1990), Figs. 8.1-8.2 Margolin and Smolarkiewicz (1998) and Figs. 10-11 Jaruga et al. (2015).

The chosen color increments correspond to the error reduction by a factor of 2, the warmer the color, the larger the error. The small gray points behind the isolines represent points for which the error value was calculated. When moving along the lines of constant Courant number, increasing the space and time discretization, number of crossed dashed isolines indicate the order of convergence. For the considered problem, it can be seen that the upwind scheme (Fig. A1) has convergence of the first order (one isoline is crossed when spatial discretization increases by one order); MPDATA scheme (Fig. A2) of the second order and MPDATA with 3 iterations (Fig. A6) is of the third order.

Moreover, the shape of the dashed isolines tells the dependency of the solution accuracy on the Courant number. When these are isotropic (truncation error being independent of polar angle), the solution is independent of the Courant number.

An interesting behavior of the schemes can be seen for Fig. A3 and Fig. A4, where the groove of the third-order convergence rate forms around $\phi = \frac{\pi}{4}$, normally characteristic for MPDATA with three or more passes. When second-order truncation error is sufficiently reduced, the third-order error, proportional to $(1 - 3C + 2C^2)$ as can be seen in (2.16), dominates, but vanishes for $C = 0.5$, thus resulting in the existence of the groove.

The convergence test result for the three-pass MPDATA with infinite gauge, non-oscillatory and third order terms options enabled (Fig. A8) are consistend with results depicted in Fig. A7, although the order of convergence is reduced due to the employment of non-oscillatory option.

*Author contributions.* The idea of the study originated in discussions between SA, SU and MO. MO led the work and preliminary version of significant part of the presented material constituted his MSc thesis prepared under mentorship of SA. PB architected the key components of PyMPDATA package. JB contributed the DPDC variant of MPDATA to PyMPDATA. MB participated in composing the paper and devising result analysis workflow. All authors contributed to the final form of the text.

*Competing interests.* The authors declare no competing interests.

*Acknowledgements.* The manuscript and the developed code benefited from comments and contributions from (in alphabetical order): Szymon Drenda, Wojciech Grabowski, Hugh Morrison, Andrzej Odrzywołek, Piotr Smolarkiewicz and Maciej Waruszewski. Paper reviews by Josef Schröttle and two anonymous reviewers helped to extend and improve the manuscript. Insider knowledge on the KiD model offered in private communications by Adrian Hill was of great help. The project was carried out with support from the Foundation for Polish Science (POIR.04.04.00-00-5E1C/18-00).

## References


Abade, G., Grabowski, W. W., and Pawlowska, H.: Broadening of Cloud Droplet Spectra through Eddy Hopping: Turbulent Entraining Parcel Simulations, J. Atmos. Sci., 75, https://doi.org/10.1175/JAS-D-18-0078.1, 2018.

Arabas, S. and Pawlowska, H.: Adaptive method of lines for multi-component aerosol condensational growth and CCN activation, Geosci. Model Dev., 4, https://doi.org/10.5194/gmd-4-15-2011, 2011.

Arabas, S. and Shima, S.-I.: Large-Eddy Simulations of Trade Wind Cumuli Using Particle-Based Microphysics with Monte Carlo Coalescence, J. Atmos. Sci., 70, https://doi.org/10.1175/JAS-D-12-0295.1, 2013.

Arabas, S. and Shima, S.-I.: On the CCN (de)activation nonlinearities, Nonlin. Proc. Geophys., 24, https://doi.org/10.5194/npg-24-535-2017, 2017.

Arabas, S., Pawlowska, H., and Grabowski, W.: Effective radius and droplet spectral width from in-situ aircraft observations in trade-wind cumuli during RICO, Geophys. Res. Lett., 36, https://doi.org/10.1029/2009GL038257, 2009.

Arabas, S., Bartman, P., and Olesik, M.: https://github.com/atmos-cloud-sim-uj/PyMPDATA, 2020.

Beason, C. W. and Margolin, L. G.: DPDC (double-pass donor cell): A second-order monotone scheme for advection, in: Fifth Nuclear Code Developers' Conference, https://www.osti.gov/servlets/purl/7049237, LLNL report UCRL-99731, 1988.

Brown, R.: A numerical study of radiation fog with an explicit formulation of the microphysics, Q. J. R. Meteorol. Soc., 106, https://doi.org/10.1002/qj.49710645010, 1980.

Chandrakar, K. K., Cantrell, W., and Shaw, R. A.: Influence of Turbulent Fluctuations on Cloud Droplet Size Dispersion and Aerosol Indirect Effects, J. Atmos. Sci., 75, https://doi.org/10.1175/JAS-D-18-0006.1, 2018.

Courant, R., Isaacson, E., and Rees, M.: On the solution of nonlinear hyperbolic differential equations by finite differences, Comm. Pure Appl. Math, 5, https://doi.org/10.1002/cpa.3160050303, 1952.

Cristiani, E.: Blending Brownian motion and heat equation, J. Coupled Syst. Multiscale Dyn., 3, https://doi.org/10.1166/jcsmd.2015.1089, 2015.

Crowley, W. P.: Numerical Advection Experiments, Mon. Weather Rev., 96, https://doi.org/10.1175/1520-0493(1968)096<0001:NAE>2.0.CO;2, 1968.

Devenish, B. J., Bartello, P., Brenguier, J.-L., Collins, L. R., Grabowski, W. W., IJzermans, R. H. A., Malinowski, S. P., Reeks, M. W., Vassilicos, J. C., Wang, L.-P., and Warhaft, Z.: Droplet growth in warm turbulent clouds, Q. J. R. Meteorol. Soc., 138, https://doi.org/10.1002/qj.1897, 2012.

Dhaniyala, S. and Wexler, A. S.: Numerical schemes to model condensation and evaporation of aerosols, Atmos. Env., 30, https://doi.org/10.1016/1352-2310(95)00288-X, 1996.

East, T. W. R.: An inherent precipitation mechanism in cumulus clouds, Q. J. R. Meteorol. Soc., 83, https://doi.org/10.1002/qj.49708335506, 1957.

Field, P., Heymsfield, A., Shipway, B., DeMott, P., Pratt, K., Rogers, D., Stith, J., and Prather, K.: Ice in Clouds Experiment–Layer Clouds. Part II: Testing Characteristics of Heterogeneous Ice Formation in Lee Wave Clouds, J. Atmos. Sci., 69, https://doi.org/10.1175/JAS-D-11-026.1, 2012.

Gettelman, A. and Morrison, H.: Advanced Two-Moment Bulk Microphysics for Global Models. Part I: Off-Line Tests and Comparison with Other Schemes, J. Climate, 28, https://doi.org/10.1175/JCLI-D-14-00102.1, 2015.

Grabowski, W. and Wang, L.-P.: Growth of Cloud Droplets in a Turbulent Environment, Annu. Rev. Fluid Mech., 45, https://doi.org/10.1146/annurev-fluid-011212-140750, 2013.

Grabowski, W., Andrejczuk, M., and Wang, L.-P.: Droplet growth in a bin warm-rain scheme with Twomey CCN activation, Atmos. Res., 99, https://doi.org/10.1016/j.atmosres.2010.10.020, 2011.

Grabowski, W. W.: Comparison of Eulerian bin and Lagrangian particle-based microphysics in simulations of nonprecipitating cumulus, J. Atmos. Sci., https://doi.org/10.1175/JAS-D-20-0100.1, 2020.

Grabowski, W. W., Morrison, H., Shima, S.-I., Abade, G. C., Dziekan, P., and Pawlowska, H.: Modeling of Cloud Microphysics: Can We Do Better?, Bull. Amer. Meteorol. Soc., 100, https://doi.org/10.1175/BAMS-D-18-0005.1, 2019.

Hall, W. D.: A Detailed Microphysical Model Within a Two-Dimensional Dynamic Framework: Model Description and Preliminary Results, J. Atmos. Sci, 37, https://doi.org/10.1175/1520-0469(1980)037<2486:ADMMWA>2.0.CO;2, 1980.

Hernandéz Pardo, L. H., Morrison, H., Machado, L. A. T., Harrington, J. Y., and Lebo, Z. J.: Drop Size Distribution Broadening Mechanisms in a Bin Microphysics Eulerian Model, J. Atmos. Sci., 77, https://doi.org/10.1175/JAS-D-20-0099.1, 2020.

Hill, A., Shipway, B., and Boutle, I.: How sensitive are aerosol-precipitation interactions to the warm rain representation?, J. Adv. Model. Earth Syst., 7, https://doi.org/10.1002/2014MS000422, 2015.

Hill, R. N.: Numerical modelling of multi-material interfaces, Ph.D. thesis, Loughborough University, https://hdl.handle.net/2134/8103, 2011.

Hirt, C. W.: Heuristic stability theory for finite-difference equations, J. Comput. Phys., https://doi.org/10.1016/0021-9991(68)90041-7, 1968.

Howell, W.: The growth of cloud drops in uniformly cooled air, J. Meteorol., 6, https://doi.org/10.1175/1520-0469(1949)006<0134:TGOCDI>2.0.CO;2, 1949.

Hulburt, H. and Katz, S.: Some problems in particle technology: A statistical mechanical formulation, Chem. Eng. Sci, 19, https://doi.org//10.1016/0009-2509(64)85047-8, 1964.

Jaruga, A., Arabas, S., Jarecka, D., Pawlowska, H., Smolarkiewicz, P. K., and Waruszewski, M.: libmpdata++ 1.0: a library of parallel MPDATA solvers for systems of generalised transport equations, Geosci. Model Dev., 8, https://doi.org/10.5194/gmd-8-1005-2015, 2015.

Jeffery, C. A., Reisner, J. M., and Andrejczuk, M.: Another Look at Stochastic Condensation for Subgrid Cloud Modeling: Adiabatic Evolution and Effects, J. Atmos. Sci., 64, https://doi.org/10.1175/2006JAS2147.1, 2007.

Khain, A. P., Beheng, K. D., Heymsfield, A., Korolev, A., Krichak, S. O., Levin, Z., Pinsky, M., Phillips, V., Prabhakaran, T., Teller, A., van den Heever, S. C., and Yano, J.-I.: Representation of microphysical processes in cloud-resolving models: Spectral (bin) microphysics versus bulk parameterization, Rev. Geophys., 53, https://doi.org/10.1002/2014RG000468, 2015.

Kostinski, A. B. and Jameson, A. R.: On the Spatial Distribution of Cloud Particles, J. Atmos. Sci., 57, https://doi.org/10.1175/1520-0469(2000)057<0901:OTSDOC>2.0.CO;2, 2000.

Kostoglou, M. and Karabelas, A. J.: Evaluation of Numerical Methods for Simulating an Evolving Particle Size Distribution in Growth Processes, Chem. Eng. Comm., 136, https://doi.org/10.1080/00986449508936360, 1995.

Kovetz, A.: An Analytical Solution for the Change of Cloud and Fog Droplet Spectra Due to Condensation, J. Atmos. Sci, 26, https://doi.org/10.1175/1520-0469(1969)026<0302:AASFTC>2.0.CO;2, 1969.

Kovetz, A. and Olund, B.: The Effect of Coalescence and Condensation on Rain Formation in a Cloud of Finite Vertical Extent, J. Atmos. Sci, 26, https://doi.org/10.1175/1520-0469(1969)026<1060:TEOCAC>2.0.CO;2, 1969.

Kühnlein, C. and Smolarkiewicz, P. K.: An unstructured-mesh finite-volume MPDATA for compressible atmospheric dynamics, J. Comp. Phys., 334, https://doi.org/10.1016/j.jcp.2016.12.054, 2017.

Kuo, H.-C., Leou, T.-M., and Williams, R. T.: A study on the high-order Smolarkiewicz methods, Comput. Fluids, 28, https://doi.org/10.1016/s0045-7930(98)00036-x, 1999.

Lange, R.: ADPIC: a three-dimensional computer code for the study of pollutant dispersal and deposition under complex conditions, https://doi.org/10.2172/4308175, LLNL report no. UCRL-51462, 1973.

Lange, R.: ADPIC—A Three-Dimensional Particle-in-Cell Model for the Dispersal of Atmospheric Pollutants and its Comparison to Regional Tracer Studies, J. Appl. Meteorol., 17, https://doi.org/10.1175/1520-0450(1978)017<0320:ATDPIC>2.0.CO;2, 1978.

Lee, H., Fridlind, A., and Ackerman, A.: An Evaluation of Size-Resolved Cloud Microphysics Scheme Numerics for Use with Radar Observations. Part II: Condensation and Evaporation, J. Atmos. Sci, 78, https://doi.org/10.1175/JAS-D-20-0213.1, 2021.

Li, X.-Y., Brandenburg, A., Haugen, N. E. L., and Svensson, G.: Eulerian and Lagrangian approaches to multidimensional condensation and collection, J. Adv. Model. Earth Syst., 9, https://doi.org/10.1002/2017MS000930, 2017.

Liu, Q., Kogan, Y. L., Lilly, D. K., and Khairoutdinov, M. P.: Variational Optimization Method for Calculation of Cloud Drop Growth in an Eulerian Drop-Size Framework, J. Atmos. Sci, 54, https://doi.org/10.1175/1520-0469(1997)054<2493:VOMFCO>2.0.CO;2, 1997.

Margolin, L. G. and Shashkov, M.: MPDATA: gauge transformations, limiters and monotonicity, Int. J. Numer. Methods Fluids, https://doi.org/10.1002/fld.1070, 2006.

Margolin, L. G. and Smolarkiewicz, P. K.: Antidiffusive Velocities for Multipass Donor Cell Advection, SIAM J. Sci. Comput., https://doi.org/10.1137/S106482759324700X, 1998.

Margolin, L. G., Shashkov, M., and Smolarkiewicz, P. K.: A discrete operator calculus for finite difference approximations, Comput. Methods Appl. Mech. Eng., https://doi.org/10.1016/S0045-7825(00)80001-8, 2000.

Morrison, H., Witte, M., Bryan, G. H., Harrington, J. Y., and Lebo, Z. J.: Broadening of Modeled Cloud Droplet Spectra Using Bin Microphysics in an Eulerian Spatial Domain, J. Atmos. Sci, 75, https://doi.org/10.1175/JAS-D-18-0055.1, 2018.

Rauber, R., Stevens, B., Ochs III, H., Knight, C., Albrecht, B., Blyth, A., Fairall, C., Jensen, J., Lasher-Trapp, S., Mayol-Bracero, O., Vali, G., Anderson, J., Baker, B., Bandy, A., Burnet, F., Brenguier, J.-L., Brewer, W., Brown, P., Chuang, P., Cotton, W., Di Girolamo, L., Geerts, H., Gerber, H., Göke, S., Gomes, L., Heikes, B., Hudson, J., Kollias, P., Lawson, R., Krueger, S., Lenschow, D., Nuijens, L., O'Sullivan, D., Rilling, R., Rogers, D., Siebesma, A., Snodgrass, E., Stith, J., Thornton, D., Tucker, S., Twohy, C., and Zuidema, P.: Rain in Shallow Cumulus Over the Ocean: The RICO Campaign, Bull. Amer. Meteorol. Soc., 88, https://doi.org/10.1175/BAMS-88-12-1912, 2007.

Roberts, K. V. and Weiss, N. O.: Convective Difference Schemes, Math. Comput., 20, https://doi.org/10.2307/2003507, 1966.

Schneider, T. Teixeira, J., Bretherton, C. S., Brient, F., Pressel, K. G., Schär, C., and Siebesma, A. P.: Climate goals and computing the future of clouds, Nat. Clim. Change, 7, https://doi.org/10.1038/nclimate3190, 2017.

Shipway, B. and Hill, A.: Diagnosis of systematic differences between multiple parametrizations of warm rain microphysics using a kinematic framework, Q. J. R. Meteorol. Soc., 138, https://doi.org/10.1002/qj.1913, 2012.

Smolarkiewicz, P. K.: A simple positive definite advection scheme with small implicit diffusion, Mon. Weather Rev., 111, https://doi.org/10.1175/1520-0493(1983)111<0479:ASPDAS>2.0.CO;2, 1983.

Smolarkiewicz, P. K.: A Fully Multidimensional Positive Definite Advection Transport Algorithm with Small Implicit Diffusion, J. Comp. Phys., 54, https://doi.org/10.1016/0021-9991(84)90121-9, 1984.

Smolarkiewicz, P. K.: Multidimensional positive definite advection transport algorithm: an overview., Int. J. Numer. Methods Fluids, 50, https://doi.org/doi:10.1002/fld.1071, 2006.

Smolarkiewicz, P. K. and Clark, T. L.: The multidimensional positive definite advection transport algorithm: Further development and applications, J. Comp. Phys., 67, https://doi.org/10.1016/0021-9991(86)90270-6, 1986.

Smolarkiewicz, P. K. and Grabowski, W. W.: The multidimensional positive definite advection transport algorithm: nonoscillatory option, J. Comp. Phys, 86, https://doi.org/10.1016/0021-9991(90)90105-A, 1990.

Smolarkiewicz, P. K. and Margolin, L. G.: On Forward-in-Time Differencing for Fluids: Extension to a Curvilinear Framework, Mon. Weather Rev., 121, https://doi.org/10.1175/1520-0493(1993)121<1847:OFITDF>2.0.CO;2, 1993.

Smolarkiewicz, P. K. and Margolin, L. G.: MPDATA – A multipass donor cell solver for geophysical flows, in: Godunov methods: Theory and applications, edited by Toro, E., Springer, https://doi.org/10.1007/978-1-4615-0663-8_81, 2001.

Smolarkiewicz, P. K. and Rasch, P. J.: Monotone Advection on the Sphere: An Eulerian Versus Semi-Lagrangian Approach, J. Atmos Sci, 48, 1991.

Smolarkiewicz, P. K. and Szmelter, J.: MPDATA: An edge-based unstructured-grid formulation, J. Comp. Phys., 206, https://doi.org/10.1016/j.jcp.2004.12.021, 2005.

Toro, E.: Riemann Solvers and Numerical Methods for Fluid Dynamics, Springer, 2 edn., https://doi.org/10.1007/b79761, 1999.

Tsang, T. H. and Brock, J. R.: Simulation of Condensation Aerosol Growth by Condensation and Evaporation, Aerosol Sci. Tech., 2, https://doi.org/10.1080/02786828308958637, 1982.

Tsang, T. H. and Korgaonkar, N.: Effect of Evaporation on the Extinction Coefficient of an Aerosol Cloud, Aerosol Sci. Tech., 7, https://doi.org/10.1080/02786828708959167, 1987.

Tsang, T. H. and Rao, A.: Comparison of Different Numerical Schemes for Condensational Growth of Aerosols, Aerosol Sci. Tech., 9, https://doi.org/10.1080/02786828808959214, 1988.

Tsang, T. H. and Rao, A.: A moving finite element method for the population balance equation, Num. Meth. Fluids, 10, https://doi.org/10.1002/fld.1650100704, 1990.

Waruszewski, M., Kühnlein, C., Pawlowska, H., and Smolarkiewicz, P. K.: MPDATA: Third-order accuracy for variable flows, J. Comput. Phys, 359, https://doi.org/10.1016/j.jcp.2018.01.005, 2018.

Wei, L., Sun, J., Lei, H., Dong, L., and Hu, W.: A Lagrangian Advection Scheme for Solving Cloud Droplet Diffusion Growth, Atmosphere, 11, https://doi.org/10.3390/atmos11060632, 2020.

Williams, M. M. R. and Loyalka, S. K.: Aerosol Science: Theory and Practice, Pergamon, 1991.

Yang, F., Kollias, P., Shaw, R. A., and Vogelmann, A. M.: Cloud droplet size distribution broadening during diffusional growth: ripening amplified by deactivation and reactivation, Atmos. Chem. Phys., 18, https://doi.org/10.5194/acp-18-7313-2018, 2018.

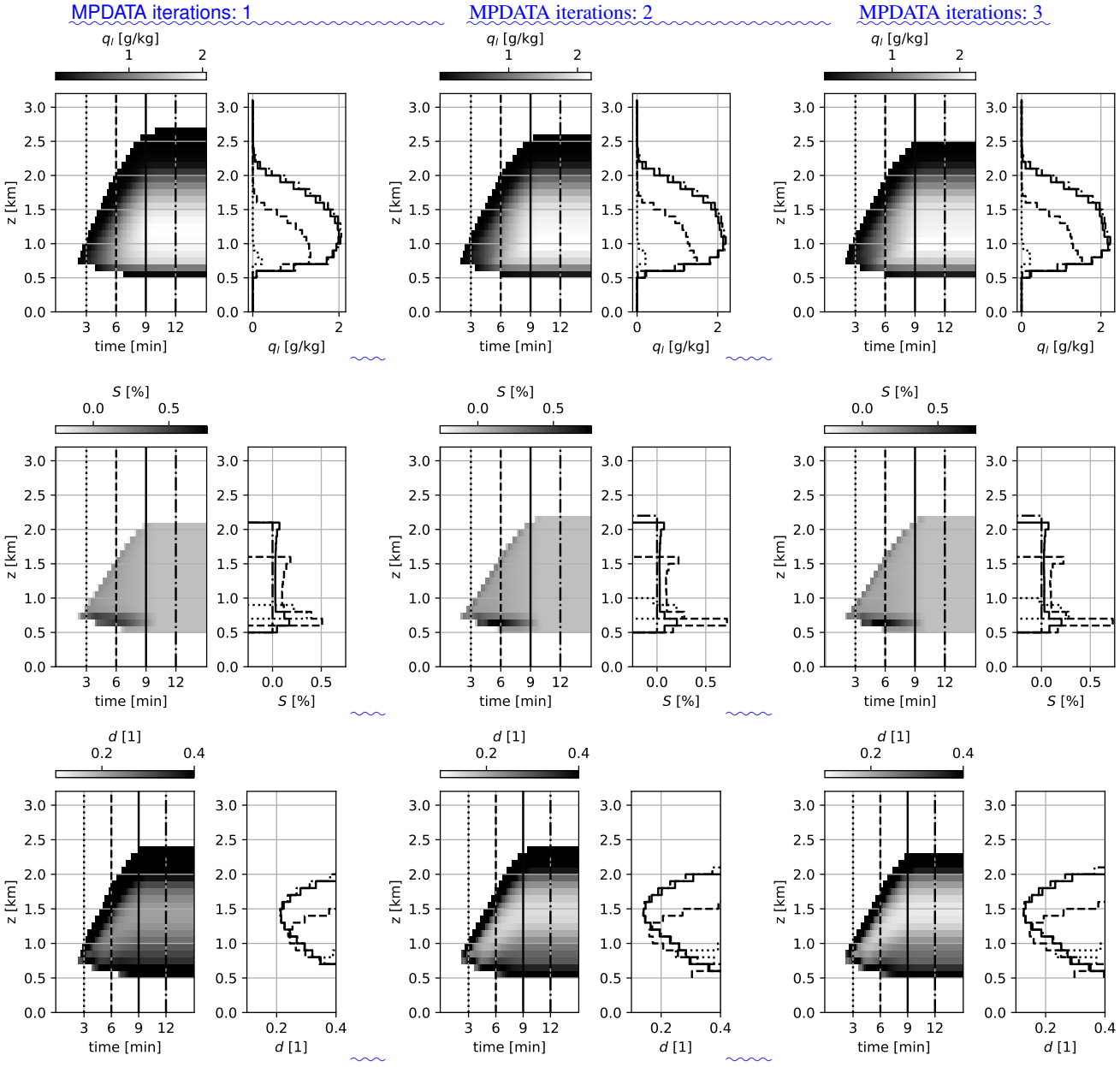


**Figure 11.** Single-column simulations depicted with three selected variables: liquid water mixing ratio $q_l$ (top row), supersaturation $S$ (middle row) and relative dispersion $d$ (bottom row); for three settings of the iteration count in MPDATA (one iteration corresponding to the basic upwind scheme, left column). Each of nine datasets (three iteration settings, three variables) is plotted with a gray-scale time vs. altitude map (left panels with color scale above) and a set of four profiles (right panels). Profiles are plotted for $t = 3$ min. (dotted), 6 min. (dashed), 9 min. (solid), & 12 min. (dash-dot), with vertical lines of corresponding line style plotted at given times in the left panels. For plotting, the model state is resampled by averaging in the time dimension to reduce the number of plotted steps by a factor of 50 (from 3600 down to 72).

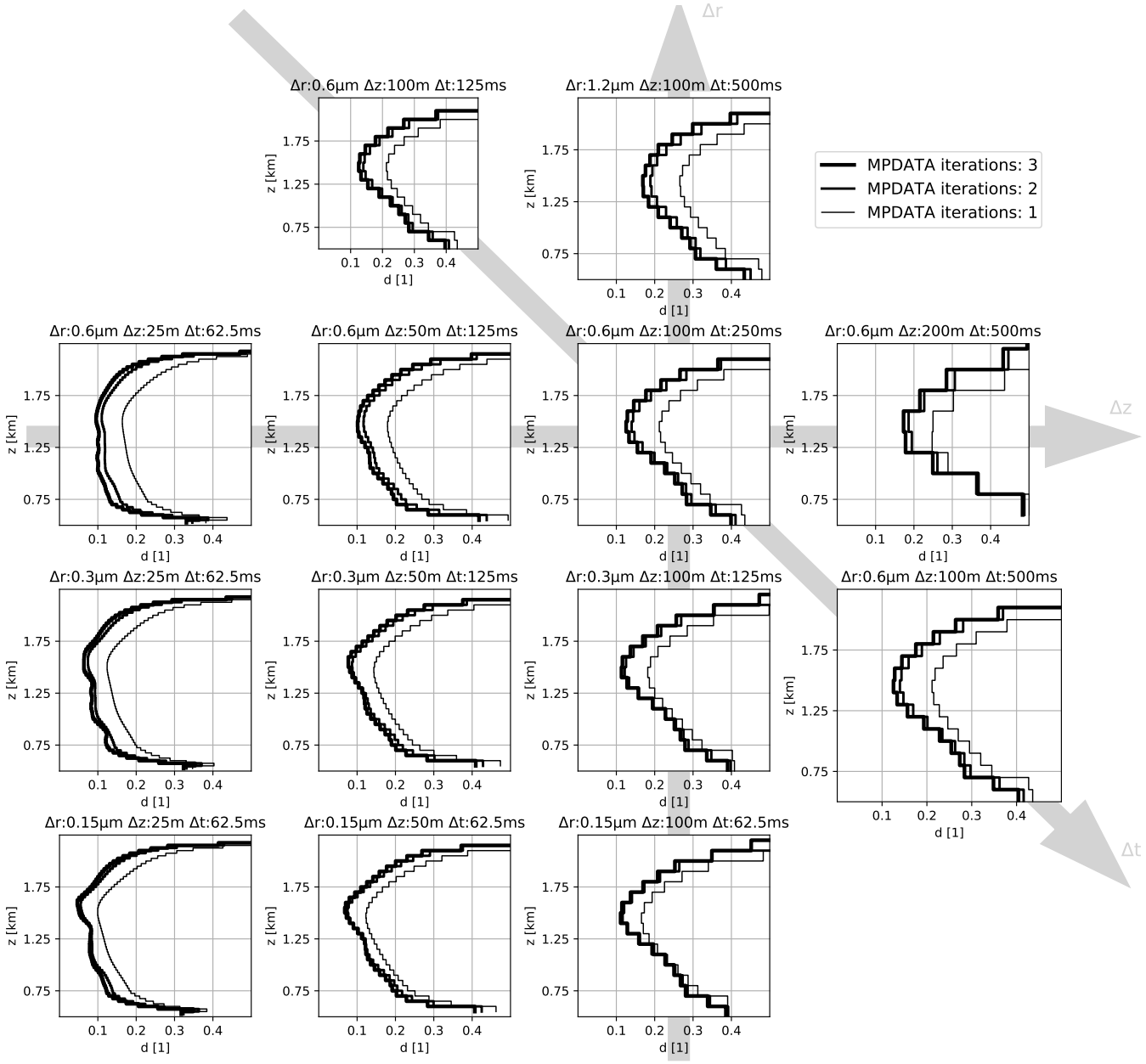


**Figure 12.** Profiles of relative dispersion $d$ for a set of temporal, spatial and spectral resolution settings ($\Delta r$, $\Delta z$ and $\Delta t$ values given in labels above each plot). Each panel depicts results for three different MPDATA iteration counts (one iteration corresponding to the basic upwind scheme). Profiles plotted for $t = t_1 = 10$ min.

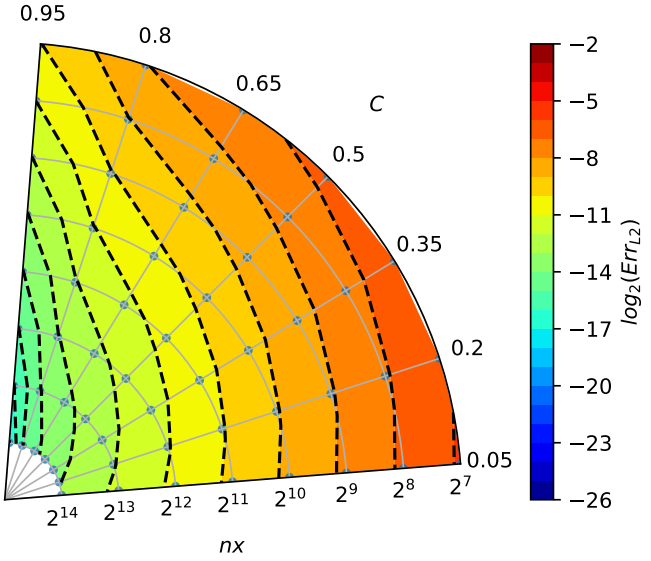


**Figure A1.** Convergence plot for the upwind scheme (cf. Fig. 1). Angle in the polar plot corresponds to the Courant number $C$; the distance from origin denotes the number of grid boxes $nx$, see eq. (A2). Gray dots indicate data point locations – parameter values for which computations were made. Colors and isolines depict the error measure values (interpolated from the data point locations), see eq. (A1).

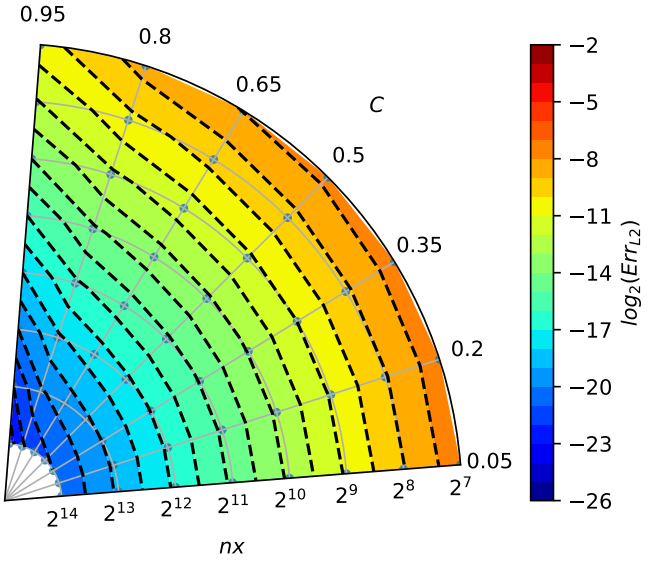


**Figure A2.** Convergence plot for basic 2-pass MPDATA (cf. Fig. 3). See caption of Fig. A1 for description of plot elements.

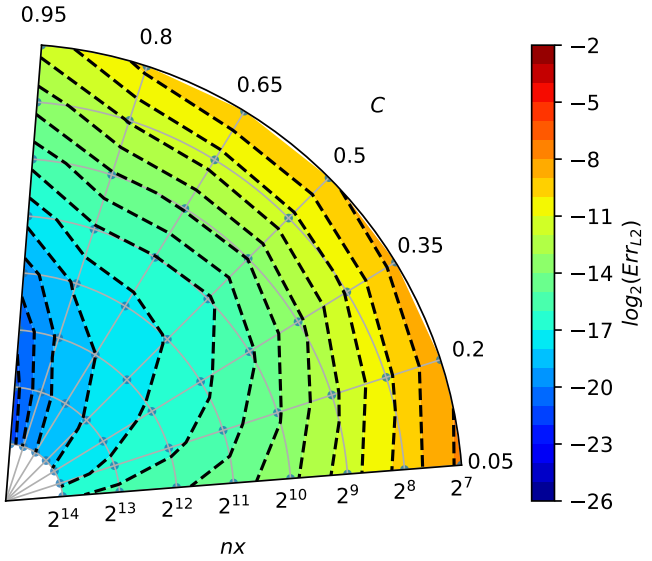


**Figure A3.** Convergence plot for the infinite gauge MPDATA (cf. Fig. 4). See caption of Fig. A1 for description of plot elements.

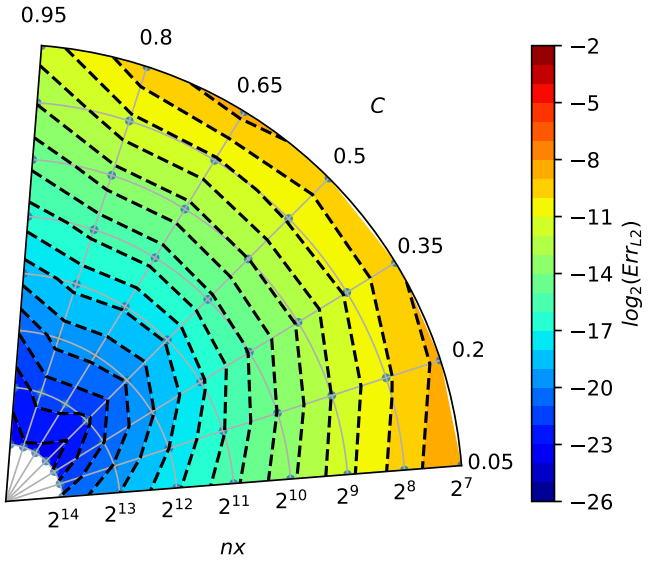


**Figure A4.** Convergence plot for the infinite gauge non-oscillatory variant of MPDATA (cf. Fig. 5). See caption of Fig. A1 for description of plot elements.

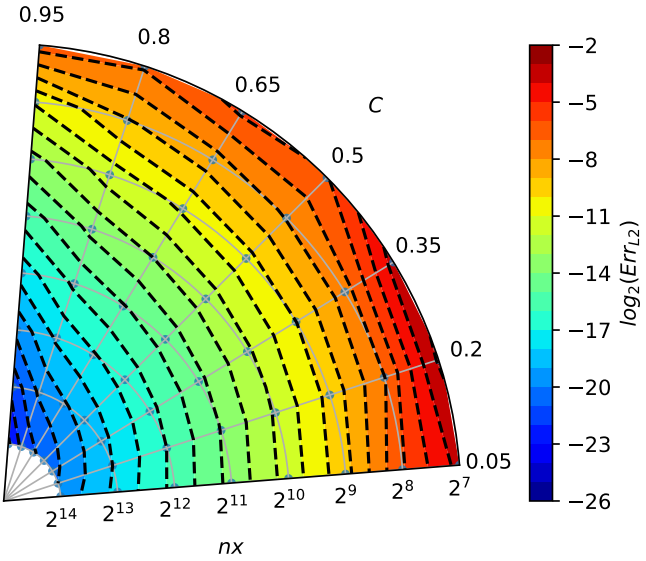


**Figure A5.** Convergence plot for the DPDC variant with infinite gauge and non-oscillatory corrections (cf. Fig. 6). See caption of Fig. A1 for description of plot elements.

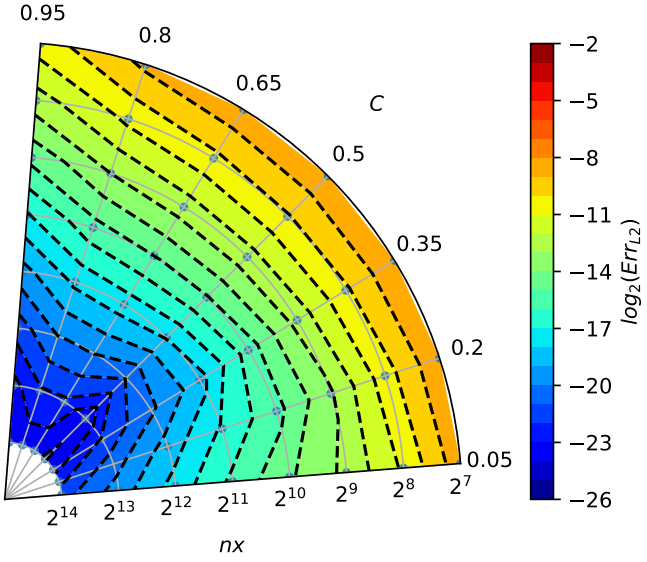


**Figure A6.** Convergence plot for the three-pass MPDATA (cf. Fig. 3). See caption of Fig. A1 for description of plot elements.

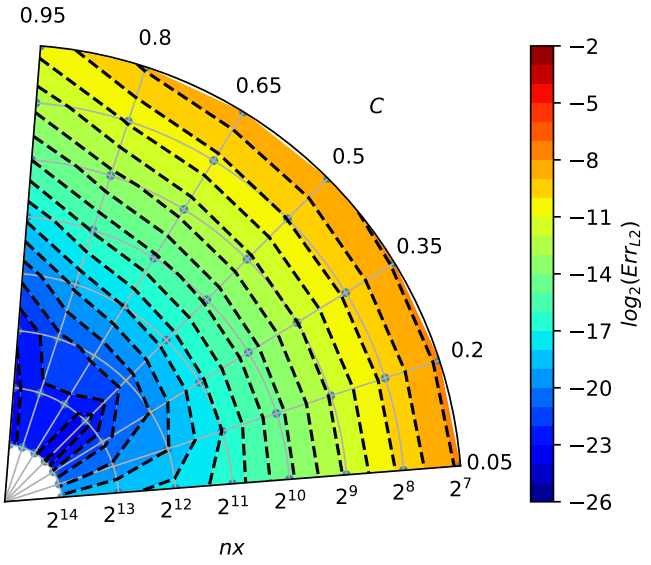


**Figure A7.** Convergence plot for the three-pass MPDATA with third order terms (cf. Fig. 7). See caption of Fig. A1 for description of plot elements.

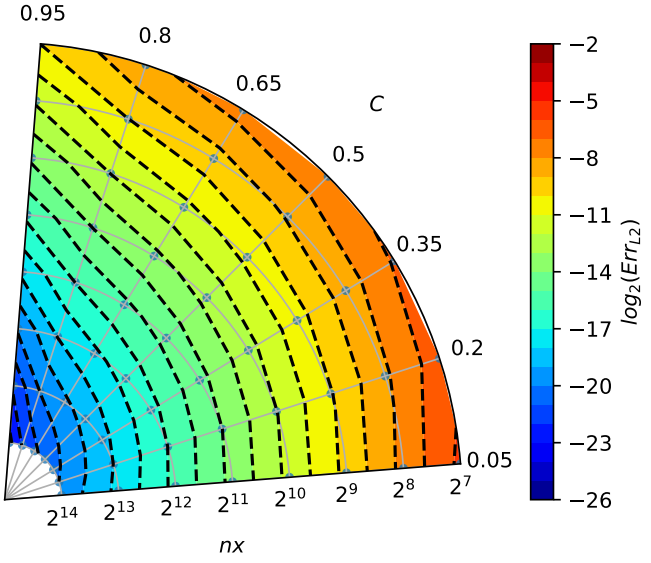


**Figure A8.** Convergence plot for the three-pass infinite gauge non-oscillatory MPDATA with third order term corrections (cf. Fig. 8). See caption of Fig. A1 for description of plot elements.